



Geochemistry, Geophysics, Geosystems



RESEARCH ARTICLE

10.1029/2021GC010071

Key Points:

- We present major and trace element and isotope data of alkaline basalts from the Plio-Quaternary Payenia volcanic province in Argentina
- Arc and intraplate geochemical signatures in Payenia lavas are explained by contributions from lithospheric mantle-derived melts
- The low-δ¹⁸O signature in olivine phenocrysts in some Payenia samples can be produced by metasomatism and melting of lithospheric mantle

Supporting Information:

Supporting Information may be found in the online version of this article.

Correspondence to:

B. H. Chilson-Parks, benjamin.chilson-parks@uconn.edu

Citation:

Chilson-Parks, B. H., Calabozo, F. M., Saal, A. E., Wang, Z., Mallick, S., Petrinovic, I. A., & Frey, F. A. (2022). The signature of metasomatized subcontinental lithospheric mantle in the basaltic magmatism of the Payenia volcanic province, Argentina. *Geochemistry, Geophysics, Geosystems*, 23, e2021GC010071. https://doi.org/10.1029/2021GC010071

Received 29 JUL 2021 Accepted 20 DEC 2021

© 2022. The Authors.

This is an open access article under the terms of the Creative Commons Attribution-NonCommercial-NoDerivs License, which permits use and distribution in any medium, provided the original work is properly cited, the use is non-commercial and no modifications or adaptations are made.

The Signature of Metasomatized Subcontinental Lithospheric Mantle in the Basaltic Magmatism of the Payenia Volcanic Province, Argentina

Benjamin H. Chilson-Parks^{1,2}, Fernando M. Calabozo³, Alberto E. Saal², Zhengrong Wang⁴, Soumen Mallick², Ivan A. Petrinovic⁵, and Frederick A. Frey⁶

¹University of Connecticut, Storrs, CT, USA, ²Brown University, Providence, RI, USA, ³Universidad Nacional de Río Negro, General Roca, Argentina, ⁴The City College of New York, New York, NY, USA, ⁵Universidad Nacional de Córdoba, Córdoba, Argentina, ⁶Massachusetts Institute of Technology, Cambridge, MA, USA

Abstract The Payenia region of Argentina (34.5–38°S) is a large Pliocene-Quaternary volcanic province of basaltic compositions in the Andean Cordillera foothills representing the northernmost extent of back-arc volcanism in the Andean Southern Volcanic Zone (SVZ). Although the chemical diversity of the Payenia basalts has been characterized previously, the processes and sources responsible for such variation remain controversial. Here, we report new whole-rock major and trace element concentrations, Sr-, Nd-, Hf-, and Pbisotope ratios and high-precision olivine oxygen-isotope ratios in a suite of 35 alkaline basalts from Payenia. These lavas have major and trace elements that define a compositional range from arc-influenced to intraplate signature. Variable crustal contamination and/or recent slab-derived inputs inadequately account for elemental and isotopic systematics and spatial compositional variations of Payenia lavas. We present a simple forward model indicating that early metasomatism and subsequent melting of the metasomatized subcontinental lithospheric mantle (SCLM) has significantly contributed to the Payenia lava compositional range. Isotopic ingrowth calculations of radiogenic Sr, Nd, Hf, and Pb suggest that the SCLM metasomatism occurred at 50-150 Ma, consistent with the timing of the breakup of Gondwana and the development of the proto-Pacific Andean arc. Variations in $\delta^{18}O_{olivine}$ values from modeled melts indicate that the metasomatism and melting within the SCLM can fractionate oxygen isotopes even when the metasomatizing melt has MORB-like δ^{18} O values, providing a different explanation for the low- δ^{18} O signatures observed in continental arc settings.

Plain Language Summary The Payenia volcanic province represents a region of the southern Andes that has remained distinctively productive in its volcanic activity over the last ~2 Ma. Much of the volcanism in Payenia is basaltic and these basalts range in composition from those that resemble volcanics erupted along the volcanic front of the Andean subduction zone to those that show little or no influence from subducted material. To better understand the causes behind the compositional diversity of Payenia basalts, this paper presents the chemical compositions of 35 basalts from various locations within Payenia. The compositions and the geographic distribution of these basalts suggest that their melt source was not solely influenced by variable amounts of subducted material interacting with the convecting mantle underneath the South American plate. Rather, significant contributions to the Payenia source may originate from the layer of mantle within the South American plate itself. In the calculations presented here, we demonstrate that the process of melting that mantle layer after it was already chemically modified by melts that stagnated in it at 50–150 Ma and then mixing it in variable amounts with a melt from the convecting mantle reproduces the compositional trends that we observe in the Payenia basalts.

1. Introduction

The Payenia volcanic province (34–38°S) is a Pliocene-Quaternary volcanic region of predominantly basaltic composition in the foreland region of the southern Mendoza and northern Neuquén provinces of western Argentina. It represents the northernmost extent of back-arc volcanism in the Andean Southern Volcanic Zone (SVZ). Payenia comprises over 800 monogenetic cinder cones, shield volcanoes (e.g., Payùn Matrù), and stratovolcanoes (e.g., Nevado and Tromen) covering roughly 40,000 km² with an estimated volcanic volume of about 8,387 km³ that is younger than 5 Ma, with most of the volcanic activity having taken place in the last ~2 Ma (Bertotto et al., 2006; Figure 1). Payenia extends from 50 to 300 km behind the volcanic front (VF), which traces the

CHILSON-PARKS ET AL. 1 of 32

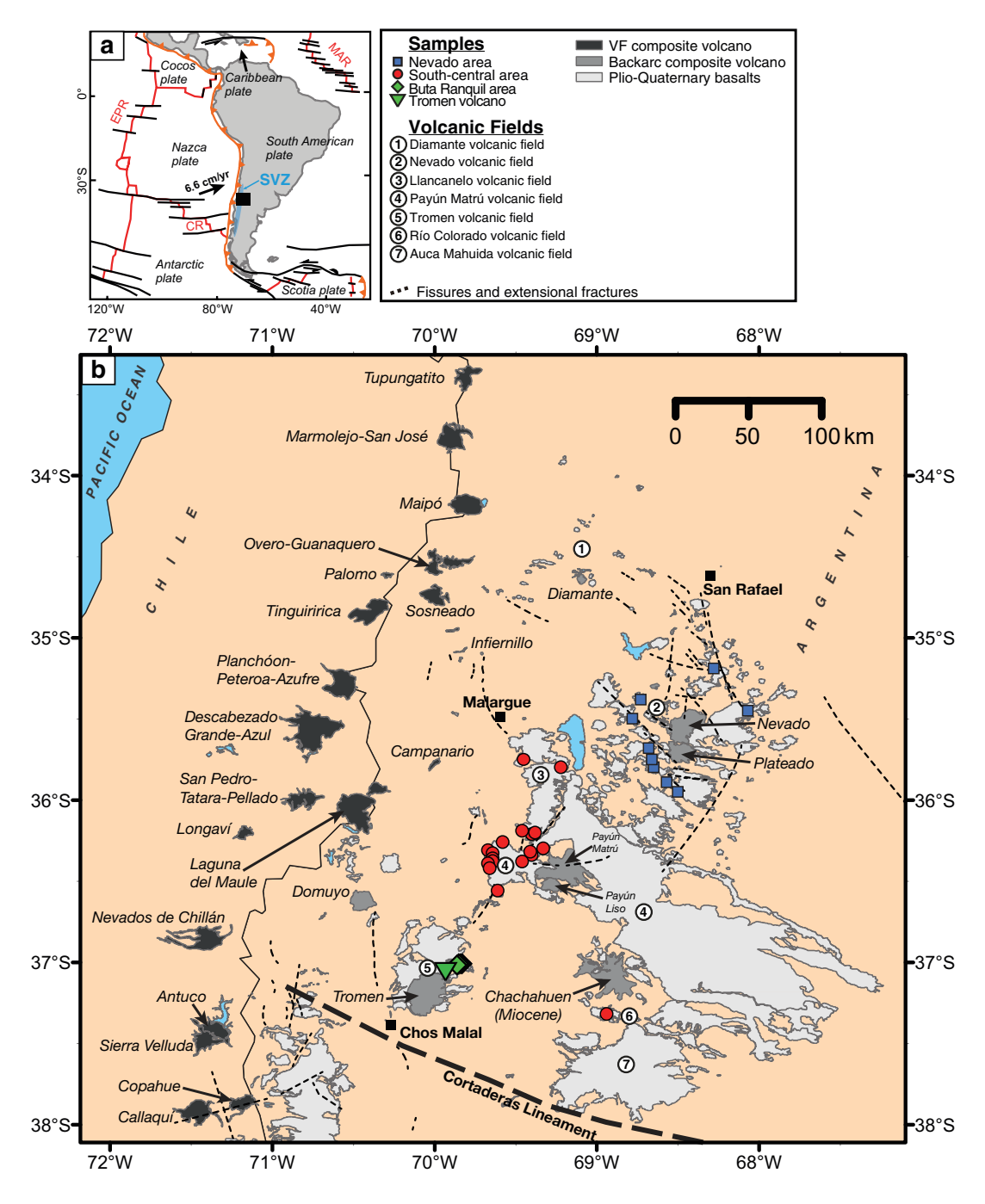


Figure 1. (a) Tectonic map of the Nazca-South America plates showing mid-ocean ridges (red lines), fracture zones (black lines), and subduction zones (orange lines with triangles). The black square marks the region displayed in part (b). Velocity and convergence direction of the Nazca-South American plates taken from Kendrick et al. (2003). Abbreviations: CR: Chile Ridge, EPR: East Pacific Rise, MAR: Mid-Atlantic Ridge, SVZ: Southern Volcanic Zone, and VF: Volcanic Front of the SVZ. (b). Simplified geologic map of the Payenia volcanic province, with locations of samples presented in this work. Note that the Payún Matrú volcanic field extends to the west and southeast of the Payún Matrú volcano and the Buta Ranquil area is smaller than the symbol size.

convergent margin between the eastwardly subducting Nazca plate and the South American Plate (\sim 66 mm/year, \sim $\overline{a}77^{\circ}$ convergence angle; Angermann et al., 1999).

The Payenia volcanic province consists of seven volcanic fields: Diamante, Nevado, Llancanelo, Payùn Matrù, Río Colorado, Tromen-Buta Ranquil, and Auca Mahuida. This province also contains several high-K calc-alkaline

CHILSON-PARKS ET AL. 2 of 32



stratovolcanoes and alkaline shield volcanoes fed by shallow magmatic chambers: the Pleisto-Holocene Payún Matrú shield volcano, the Plio-Pleistocene Cerro Nevado, Domuyo, Tromen volcanoes, the Pleistocene Auca Mahuida basaltic shield, and the Miocene Chachahuén volcano (Figure 1; Ramos & Folguera, 2011 and references therein).

Payenia occupies a region of South America formed by Paleozoic accretion of mid-late Mesoproterozoic terranes (Chilenia and Cuyania) during the amalgamation of Gondwana (Ramos, 2004, 2010 and references therein). The Mesozoic breakup of Gondwana and formation of the Atlantic Ocean is associated with a period of continental extension that formed sedimentary basins in the east and compression responsible for the proto-Andes in the west. Toward its northern extent, Payenia covers a partially deformed sedimentary basin characterized by a 1000-m-thick undifferentiated Cenozoic sequence and toward its southern extent it covers upper Cretaceous to lower Paleogene sediments of the Neuquén basin (Folguera et al., 2009; Kay, Burns, et al., 2006). The northern and eastern extent of Payenia, which includes the Nevado and Diamante volcanic fields (Figure 1), sits on top of the San Rafael Block, which represents an uplifted portion of the Mesoproterozoic Cuyania terrane, as well as the fold and thrust belt of the Andean Principal Cordillera foothills. Western and southern Payenia sits on Cenozoic sediments and poorly exposed Mesoproterozoic basement (Cingolani, Basei et al., 2017; Ramos, 2004, 2010 and references therein).

The mid-late Miocene period represents an important time of deformation of the Payenia province. It is characterized by crustal thickening, uplift of the San Rafael Block and the eastward expansion and migration of the volcanic arc, and formation of high-K calc-alkaline stratovolcanoes. These observations have been interpreted as a transient episode of shallow subduction of the Nazca slab (Kay et al., 2004, Kay, Burns et al., 2006, Kay, Mancilla, & Copeland, 2006). The onset of Payenia basaltic volcanism and subsequent period of extension, which is evidenced by normal faulting of the Late Miocene uplifted peneplain of the San Rafael Block, are associated with the steepening of the subducted slab (Ramos & Folguera, 2011 and references therein).

Previous investigations into the source of Payenia alkaline basalts noted their large compositional variation, ranging from typical arc to intraplate magmatism (Germa et al., 2010; Gudnason et al., 2012; Hernando et al., 2014; Jacques et al., 2013; Kay, Burns et al., 2006, 2013; Pallares et al., 2016; Stern et al., 1990; Søager & Holm, 2013; Søager et al., 2013, Søager, Holm & Thirlwall, 2015). Although the chemical diversity of the Payenia basalts has been characterized previously, the processes and sources responsible for such variation remain controversial. Stern et al. (1990) categorized the chemical diversity of Patagonia back-arc magmatism, including the Payenia province, into two main groups named "transitional" and "cratonic" basalts. Transitional basalts are back-arc lavas that, relative to VF basalts, have similar radiogenic isotopes but less dramatic enrichments in large-ion lithophile elements (LILEs) relative to high-field-strength elements (HFSEs) contents. In contrast, cratonic basalts have incompatible trace element and radiogenic isotopic compositions significantly different from the VF lavas, but within the compositional range of oceanic island basalts. Stern et al. (1990) also noted that transitional basalts erupted closer to the VF, whereas cratonic basalts erupted farther to the east, indicating a weakening of the arc signature away from the VF. Transitional back-arc basalts are considered representative of the melting of the mantle wedge with a weaker slab-derived fluid/melt flux than beneath the VF, whereas cratonic basalts represent lower-degree melts of heterogeneous asthenosphere unaffected by subduction processes. Although variable involvement of metasomatized sub-continental lithospheric mantle (SCLM) has been considered likely in both "transitional" and "cratonic" basalts, its role in the composition of these lavas has not been clearly defined.

More recent studies have not provided a clearer picture of the processes and sources responsible for the chemical diversity of Payenia lavas. The most accepted process behind the triggering of Payenia volcanism is extension due to trench roll-back following steepening of a flat slab that existed in the middle to late Miocene (Kay et al., 2004, Kay, Burns et al., 2006, Kay, Mancilla, & Copeland, 2006). However, to explain the large compositional range of Payenia lavas, different studies have invoked different sources of the volcanism. Among the most commonly cited sources are mixed peridotite-pyroxenite asthenosphere within the mantle wedge beneath Payenia that was variably affected by subduction process (Søager & Holm, 2013; Søager et al., 2013, Søager, Holm, & Thirlwall, 2015, Søager, Portnyagin et al., 2015) and the heating and melting of a previously metasomatized sub-continental lithospheric mantle (SCLM; Jacques et al., 2013; Kay et al., 2013; Søager et al., 2018). Although the Payenia basalts can be explained by a heterogeneous peridotite-pyroxenite asthenosphere mantle wedge variably affected by subduction processes, such a process cannot explain the geographic distribution of lava compositions across the different volcanic fields. Therefore, other processes or sources must be considered to explain this occurrence.

CHILSON-PARKS ET AL. 3 of 32



Here, we report new whole-rock major and trace element concentrations, Sr, Nd, Hf, and Pb isotopes, and olivine phenocryst δ^{18} O values of 35 basaltic lavas sampled from the Payenia volcanic province to better define the sources of the mafic volcanism and their geographic distribution. Lavas were preferentially sampled from smaller, monogenetic eruptive centers in contrast to material erupted from large stratovolcanoes because they are relatively primitive (i.e., higher MgO contents), and are not associated with large magma chambers, meaning they are minimally affected by crustal contamination and shallow-level processes and provide more faithful information on the "primary" compositional variation than stratovolcano eruptive products. The geochemical signatures of the sampled lavas bear a close resemblance to those found in metasomatized mantle xenoliths from the Patagonian back-arc, leading us to recognize that the melting of the SCLM represents a viable control on the distribution and compositional variation of mafic volcanism within Payenia. We test this hypothesis with a forward model that considers mantle wedge basalts modified by melts generated from previously metasomatized SCLM; such a model reproduces the geochemical traits of Payenia lavas.

2. Methods

We analyzed whole-rock powders for major and trace element concentrations and Sr, Nd, Pb, and Hf isotopes, and olivine phenocrysts for oxygen isotope ratios (Table S1). Whole-rock major element oxide (SiO₂, TiO₂, Al₂O₃, FeO^T, CaO, MgO, MnO, K₂O, Na₂O, and P₂O₅) and some trace element (Cr, V, Ni, Zn, and Ga) concentrations were measured by X-ray fluorescence (XRF) spectrometry using a Siemens XRF spectrometer at the University of Massachusetts, Amherst, except for samples MEN-026 and VEJ-041. Average precision in most major elements yielded <1.5% RSD (2 σ) for duplicated sample analyses. V, Zn, Ga, Ni, and Cr concentrations yield 2 σ average standard deviations of 1.8%, 1%, 3.8%, 7%, and 2.6%, respectively. The large error in Ni indicates the effect of inhomogeneity of the sample aliquots.

For samples MEN-026 and VEJ-041, XRF analyses of the same set of major and trace elements were performed at the Peter Hooper GeoAnalytical Lab, Washington State University (WSU) by a ThermoARL Advant'XP + sequential XRF spectrometer. Sample preparation, analytical procedure, accuracy, and precision are detailed in Johnson et al. (1999). To monitor instrumental drift, analyses of GSP2, BCR-1, and AGV-2 standards were performed every 24–48 hr, with a precision of 0.2%-1% 2σ RSD. Analyses of 5 sets of duplicate beads of whole-rock sample powders yielded a reproducibility of <2% 2σ RSD for all major elements except MnO (<2.2%) and MgO (<2.5%). V, Zn, Ga, Ni, and Cr concentrations from these duplicate beads yield 2σ average standard deviations of 1.1%, 2.8%, 8.8%, 3.4%, and 0.4%, respectively.

For all samples, the remaining trace elements (Sc, Rb, Sr, Y, Zr, Nb, Cs, REE, Th, U, Hf, Ta, and Pb) were measured on Li-tetraborate fused beads by inductively coupled plasma-mass spectrometry (ICP-MS) using an Agilent 7700 quadrupole mass spectrometer at WSU. Reproducibility over the course of the analyses was assessed by repeatedly measuring the compositions of an international rock standard (BCR-2, n = 54), an in-house standard (TED, n = 33) as unknowns among the samples. Precision yielded <5% RSD (2 σ) for most elements except for Pb in BCR-2 (<8%) and Cs in TED (<12%). In addition to monitoring trace element reproducibility with the BCR-2 and TED standards, trace element concentrations of an alkaline basalt sample from the Nevado volcanic field were measured five times during the course of the analyses, yielding <6% RSD (2 σ) for most elements except for Pb (<28%) and Sc (<8%).

Sr, Nd, Hf, and Pb isotopic compositions were measured on a Thermo Scientific Neptune Plus MC-ICP-MS at the Mass Spectrometer Analytical Facility, Brown University. Sr, Nd, and Hf were introduced in the plasma using a PFA nebulizer with a flow rate of ~70 μ L/min coupled with a glass spray chamber, while Pb was introduced with an APEX-IR introduction system to enhance the sensitivity. The mass spectrometer was equipped with an H-skimmer cone and H-sampler cone. The baseline measurement was taken at -0.5 amu. 87 Sr/ 86 Sr, 143 Nd/ 144 Nd, and 176 Hf/ 177 Hf ratios were corrected for instrumental mass fractionation using an 88 Sr/ 86 Sr = 0.1194, 146 Nd/ 144 Nd = 0.7219, and 179 Hf/ 177 Hf = 0.7325, respectively, with an exponential law. Pb solution was spiked with NBS SRM-997 Tl standard prior to the analysis with a Pb/Tl = 4 to correct for the mass fractionation using an exponential law with 203 Tl/ 205 Tl = 0.418922. Sr, Nd, and Hf were measured at 200 ppb concentration whereas Pb was measured at 75 ppb concentration level. 87 Sr/ 86 Sr, 143 Nd/ 144 Nd, and 176 Hf/ 177 Hf ratios of samples are reported relative to the NBS SRM 987 standard with 87 Sr/ 86 Sr = 0.71024, the JNd-i standard with 143 Nd/ 144 Nd = 0.512115, and the JMC-475 standard with 176 Hf/ 177 Hf = 0.282160, respectively. 206 Pb/ 204 Pb, and 208 Pb/ 204 Pb

CHILSON-PARKS ET AL. 4 of 32



ratios are reported relative to the NBS 981 standard with $^{206}\text{Pb}/^{204}\text{Pb} = 16.9356$, $^{207}\text{Pb}/^{204}\text{Pb} = 15.4891$, and $^{208}\text{Pb}/^{204}\text{Pb} = 36.7006$ (Todt et al., 1996). The internal precision is 5–10 ppm for Sr and Nd, 20–45 ppm for Pb, and 20–30 ppm for Hf, while the external precision over the course of two years is 27 ppm for Sr (2σ , n = 75), 29 ppm for Nd (2σ , n = 104), 39 ppm for Hf (2σ , n = 89), and 100 ppm for Pb isotopes (2σ , n = 75). Procedure blanks were <50 pg for Sr and Pb and <30 pg for Nd and Hf. The USGS reference material BCR-2 and BIR-1 were processed during the sample preparation and measured with the same instrument set up, data for both are consistent with the range reported in GeoRem database.

Oxygen isotope analyses of olivine phenocrysts were measured by the infrared-laser fluorination technique at Yale University, using previously described methods (Eiler et al., 1996). During analysis, measurements of standards UWG (Gore Mountain garnet from New York) and KHX-1 (Kilbourne Hole olivine from New Mexico) were interspersed with measurements of unknown samples. Results for the standards are UWG-2 = $5.77 \pm 0.14\%$ (n = 16) and KHX-1 = $5.20 \pm 0.13\%$ (n = 38), which are within the analytical uncertainty of accepted values of UWG (5.80%) and KHX-1 (5.25%; Eiler, Crawford et al., 2000, Eiler, Schiano et al., 2000; Valley et al., 1995; Wang et al., 2011). All standard deviations refer to 1σ of long-term reproducibility of raw measurements. All δ^{18} O values for unknown samples on a given day were corrected by the difference between measured and accepted values for standards on that day. Standard deviations typically were <0.1% for samples with duplicated measurements.

Additional details concerning petrography, melt-olivine equilibrium, sample preparation, and analytical methods can be found in the Supporting Information S1.

3. Results

Hereafter, we refer to three areas of the Payenia volcanic province (Figure 1). The Buta Ranquil area represents the small eruptive centers at the Buta Ranquil locality and the Tromen stratovolcano. The south-central area is comprised of the Llancanelo, Payún Matrú, Auca Mahuida, and Río Colorado volcanic fields (data from the Auca Mahuida volcanic field are only represented by previously published studies). The Nevado area contains the Nevado volcanic field, Diamante volcanic field, and back-arc stratovolcanoes Cerro Nevado and Cerro Diamante.

3.1. Major and Trace Element Concentrations

Major and trace element concentrations are reported in Table S1. Most of the samples range from alkali basalt to trachybasalts with two samples from the Buta Ranquil region ranging to basaltic trachyandesite (Figure 2). All but six samples in this study are nepheline-normative according to the CIPW norm classification, while two from the Nevado and four from the Buta Ranquil areas are hypersthene-normative (Table S1). MgO and SiO₂ concentrations for the samples vary from 5 to 12 wt.% and from 46.0 to 52.5 wt.%, respectively, except for the hy-normative basaltic trachyandesite sample 27–5, taken from a flow on the northeastern flank of the Tromen volcano, which has 55.4 wt.% SiO₂ (Figure 3). The observed compositional range resembles what was previously reported for Payenia samples (Hernando et al., 2014; Jacques et al., 2013; Søager et al., 2013). Relative to lavas from the VF at the same latitude, the lavas from the Payenia volcanic province range to lower SiO₂, Al₂O₃, higher FeO^T, CaO, TiO₂, P₂O₅, Na₂O, and K₂O at a given MgO content (Figure 3).

A comparison of lavas from the different areas within Payenia show that Nevado area lavas have on average higher MgO contents than those of Buta Ranquil and south-central basalts. Sample 27–5, from the Tromen volcano, exhibits major element concentrations like those of the VF lavas. Other Buta Ranquil lavas span a range in major element concentrations between Tromen and south-central lavas.

Trace element patterns of lavas from the Nevado and Buta Ranquil areas share similarities with VF lavas not significantly affected by crystal fractionation (Figures 4a and 4b); they have a typical arc signature (high LILE/HFSE ratios), but with higher concentrations of incompatible trace elements and relatively smaller Nb, Ta, and Ti negative anomalies in primitive mantle normalized diagrams (i.e., the "transitional" lavas of Stern et al., 1990). The trace elements of south-central lavas lack or have a minimal arc signature (Figure 4c); their trace element patterns more closely resemble those of intraplate basalts, which lack depletions in Nb, Ta, and Ti relative to elements of similar incompatibility during mantle melting (i.e., the "cratonic" lavas of Stern et al., 1990).

CHILSON-PARKS ET AL. 5 of 32

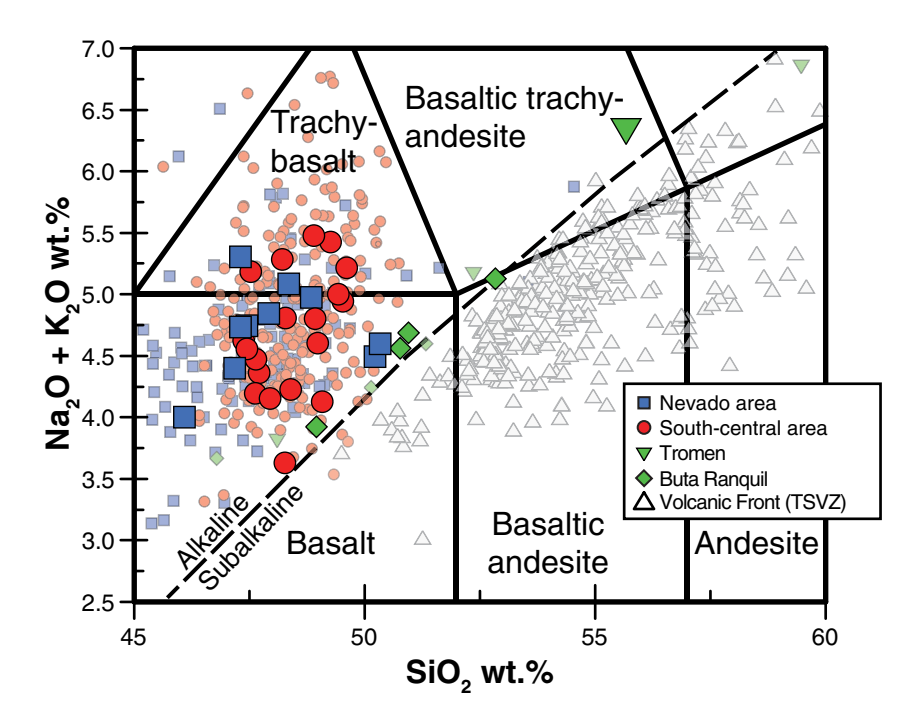


Figure 2. Total alkali versus silica diagram (TAS, Le Bas et al., 1986) of Payenia and VF samples, using the same symbols as in Figure 1. Black dashed line separates the alkaline (above the line) from the subalkaline fields (MacDonald & Katsura, 1964). Payenia literature data (smaller semitransparent symbols) from Germa et al. (2010); Gudnason et al. (2012); Hernando et al. (2014); Jacques et al. (2013); Kay, Burns, et al. (2006); Kay et al. (2013); Pallares et al. (2016); Søager and Holm (2013); Søager et al. (2013); Søager, Holm, and Thirlwall, 2015. VF literature data from Davidson et al. (1988); Dungan et al. (2001); Ferguson et al. (1992); Holm et al. (2014); Jacques et al. (2013); Rodríguez et al. (2007); Ruprecht et al. (2012); Sellés et al. (2004); Tormey et al. (1995).

3.2. Sr-Nd-Pb-Hf Isotopes of Whole-Rock Powders

Newly obtained Sr-Nd-Pb-Hf isotope ratios are reported in Table S1 and Figure 5. Our data cover a similar range to what has been previously reported for Payenia lava samples (Holm et al., 2014, 2016; Jacques et al., 2013; Kay, Burns et al., 2006, 2013; Saal, 1994; Søager & Holm, 2013; Søager et al., 2013, Søager, Holm, & Thirlwall, 2015). The ⁸⁷Sr/⁸⁶Sr and ¹⁴³Nd/¹⁴⁴Nd ratios for Payenia lavas are negatively correlated (Figures 5a and 5b) and overlap with values reported for VF lavas (Davidson et al., 1987; Harmon et al., 1984; Hickey et al., 1986; Hildreth & Moorbath, 1988; Tormey et al., 1995). Both Payenia and VF lavas have ⁸⁷Sr/⁸⁶Sr and ¹⁴³Nd/¹⁴⁴Nd ratios within the range reported for the Discovery and Shona segments of the southern Mid-Atlantic Ridge (MAR), similar to higher ¹⁴³Nd/¹⁴⁴Nd and lower ⁸⁷Sr/⁸⁶Sr values than those of Chile Trench sediments, and significantly lower ¹⁴³Nd/¹⁴⁴Nd and ⁸⁷Sr/⁸⁶Sr values than the Nazca metalliferous sediments. East Pacific Rise (EPR) MORBs (Gale et al., 2013) yield significantly higher ¹⁴³Nd/¹⁴⁴Nd and lower ⁸⁷Sr/⁸⁶Sr values than those for Andean volcanics. Metamorphic and magmatic basement rocks from the regions surrounding Payenia have significantly lower ¹⁴³Nd/¹⁴⁴Nd values and most have significantly higher ⁸⁷Sr/⁸⁶Sr values than Payenia lavas.

 $^{176} Hf/^{177} Hf$ versus $^{143} Nd/^{144} Nd$ values are positively correlated (Figure 5c), however, Payenia lavas generally have lower $^{176} Hf/^{177} Hf$ at similar $^{143} Nd/^{144} Nd$ values than those of VF lavas and trench sediments. Payenia lavas display a range in $^{176} Hf/^{177} Hf$ ratios that extend from values similar to the mantle array (Chauvel et al., 2008) to values below the array (i.e., $\Delta\epsilon_{Hf} < 0$). Most Payenia lavas have Nd and Hf isotope values distinct from the Discovery-and Shona-influenced MAR MORBs. EPR MORBs yield higher $^{143} Nd/^{144} Nd$ and $^{176} Hf/^{177} Hf$ ratios than Andean volcanics. The two hypersthene-normative Nevado area samples have lower $^{143} Nd/^{144} Nd$ and $^{176} Hf/^{177} Hf$ and higher $^{86} Sr/^{87} Sr$ values than the nepheline-normative samples from the same area. In contrast, in the Buta Ranquil area, the hypersthene-normative samples have higher $^{143} Nd/^{144} Nd$ and $^{176} Hf/^{177} Hf$ and lower $^{86} Sr/^{87} Sr$ values than the nepheline-normative ones. These distinctions in isotope ratios suggest that the processes responsible for hypersthene-normative lavas in the Nevado area might differ from those in the Buta Ranquil region.

CHILSON-PARKS ET AL. 6 of 32



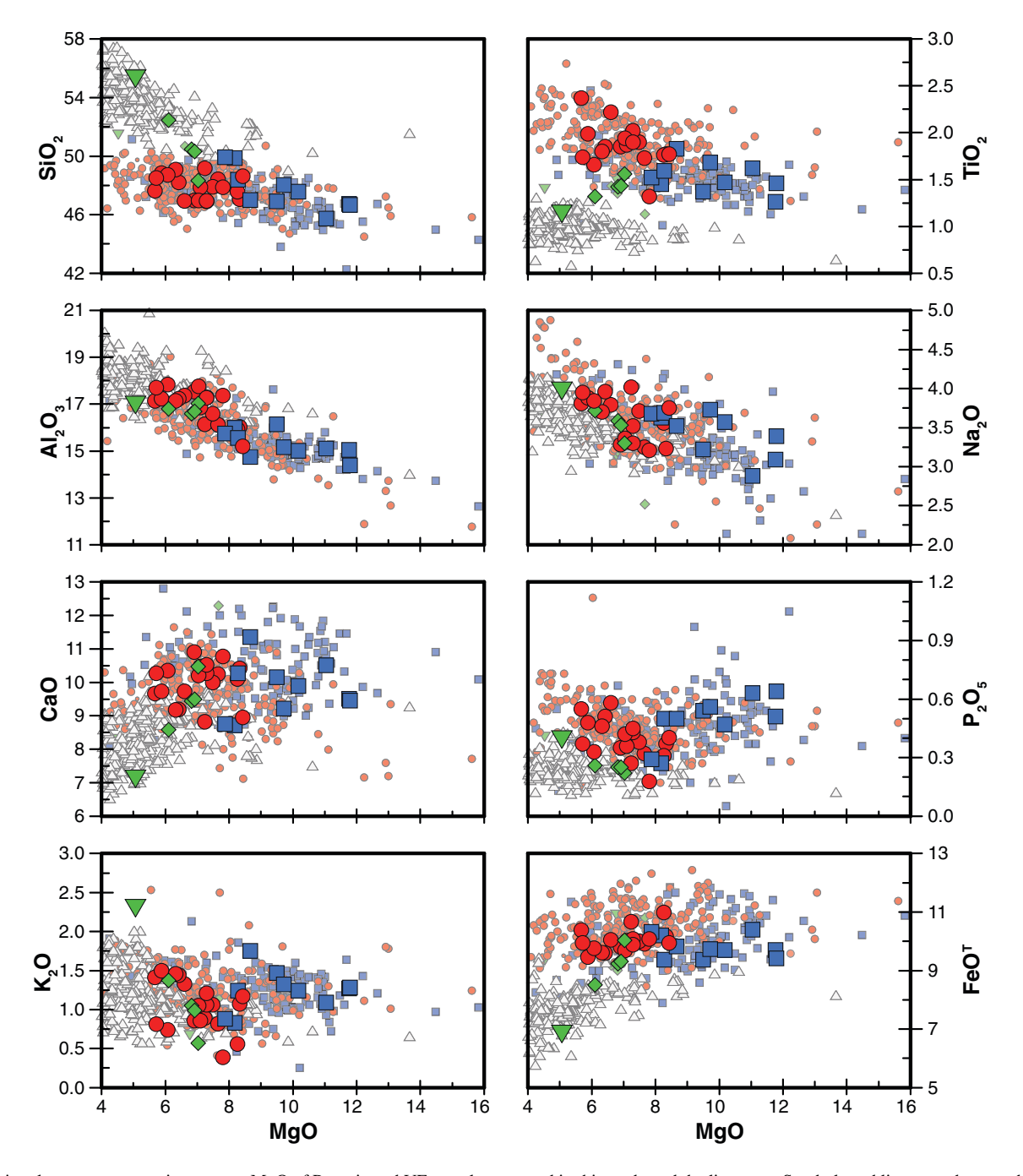


Figure 3. Major element concentrations versus MgO of Payenia and VF samples reported in this study and the literature. Symbols and literature data are the same as in Figure 2.

Pb isotopes for Payenia volcanic province and VF lavas show strong positive correlations that span a range of values between those for Discovery-Shona MAR MORBs and for Chile Trench sediments (Figures 5d–5g). The south-central lavas have the least radiogenic Pb compositions in Payenia, which overlap with the range of isotope values of Discovery-Shona MAR MORBs. The Nevado and Buta Ranquil area lavas span a range in ²⁰⁶Pb/²⁰⁴Pb values between those of south-central lavas and VF lavas influenced by trench sediment. Paleozoic to Cenozoic basement rocks that occur at latitudes 36-41°S generally exhibit higher ²⁰⁷Pb/²⁰⁴Pb and ²⁰⁸Pb/²⁰⁴Pb values at a

CHILSON-PARKS ET AL. 7 of 32

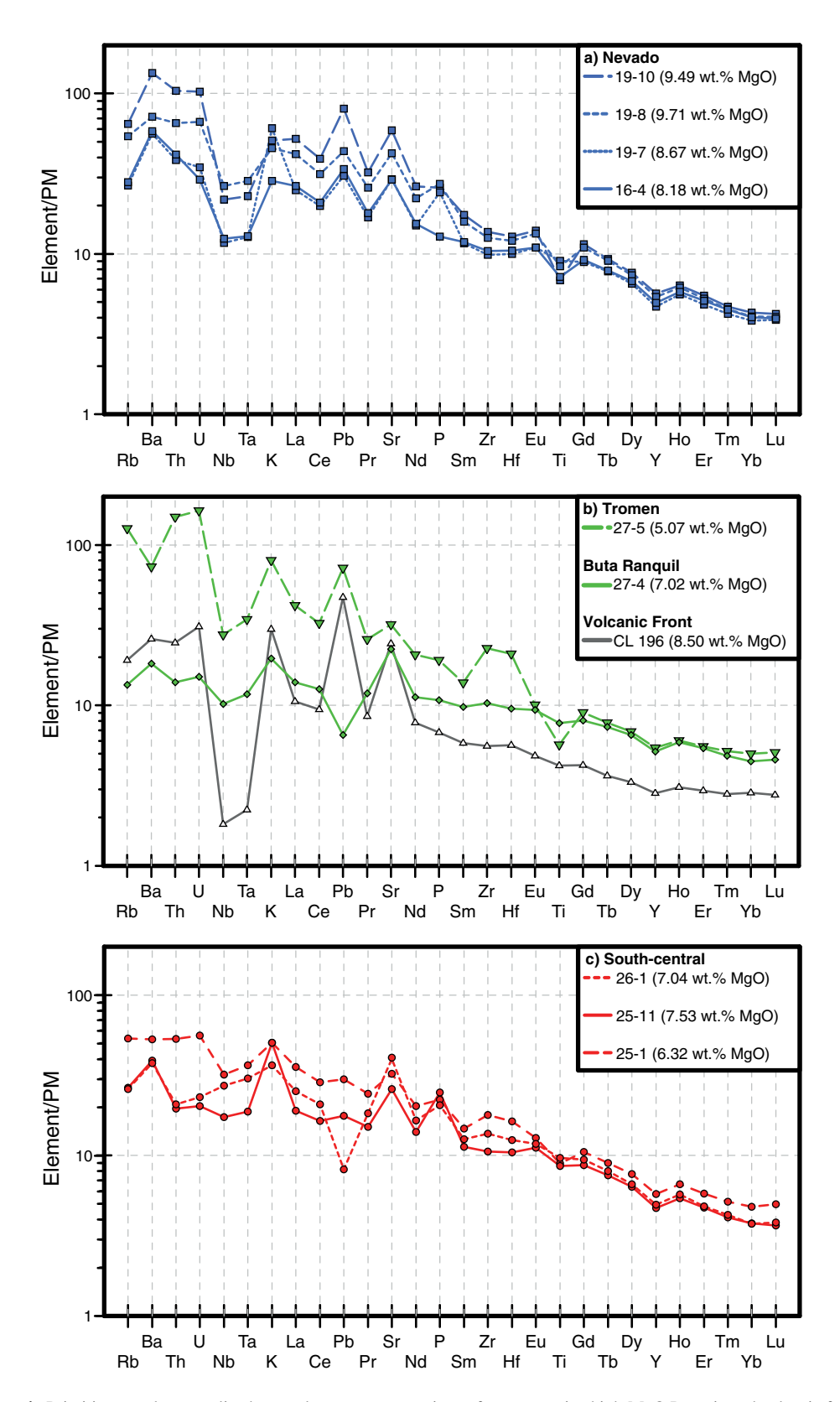


Figure 4. Primitive mantle-normalized trace element concentrations of representative high-MgO Payenia and volcanic front lavas. Sample CL196 is representative of the VF from Jacques et al. (2013). Normalization values from McDonough and Sun (1995).

CHILSON-PARKS ET AL. 8 of 32



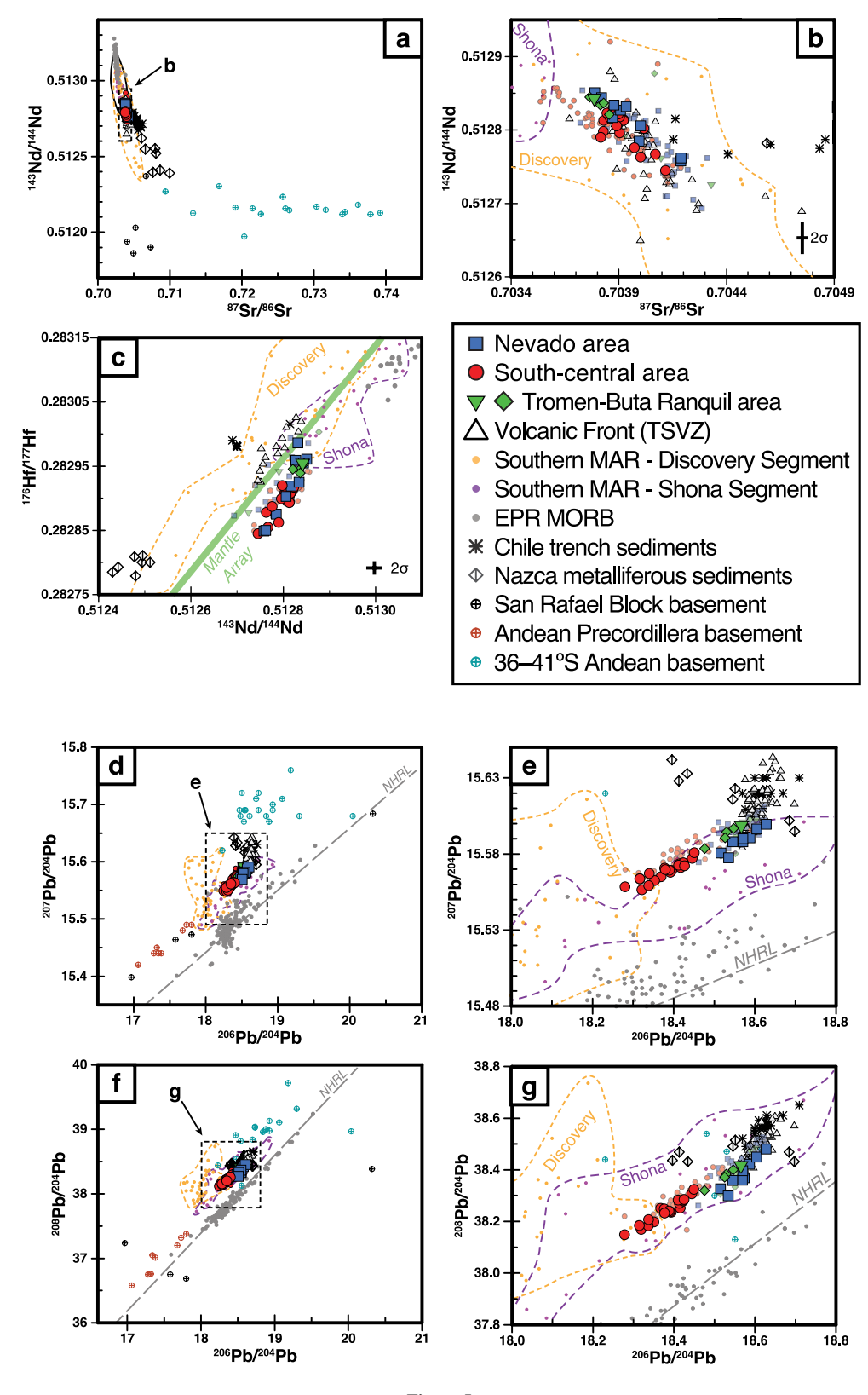


Figure 5.

CHILSON-PARKS ET AL. 9 of 32



given $^{206}\text{Pb}/^{204}\text{Pb}$ value relative to those of Payenia, VF, and trench sediment samples. Mesoproterozoic basement rocks from the San Rafael Block and the Andean Precordillera occur at significantly lower $^{206}\text{Pb}/^{204}\text{Pb}$, and $^{208}\text{Pb}/^{204}\text{Pb}$ values than Payenia samples, except for one crustal xenolith sample from the Precordillera, which has higher $^{206}\text{Pb}/^{204}\text{Pb}$ but significantly lower $\Delta 7/4$ and $\Delta 8/4$ values (Figures 5d and 5f). Among the Payenia groups, Nevado area lavas have relatively low $\Delta 8/4$ values, defining a trend distinct from the one defined by Buta Ranquil and south-central samples, which exhibit intermediate and high $\Delta 8/4$ values, respectively (Figures 5e and 5g). EPR MORB samples occur along the Northern Hemisphere Reference Line (Hart, 1984), which has significantly lower $^{207}\text{Pb}/^{204}\text{Pb}$ and $^{208}\text{Pb}/^{204}\text{Pb}$ values at a given $^{206}\text{Pb}/^{204}\text{Pb}$ value than the Payenia samples.

3.3. Oxygen Isotopes of Olivine Phenocrysts

The $\delta^{18}O$ values of olivine phenocrysts from Payenia lavas range from 4.84 to 5.39% (Table S1). This $\delta^{18}O_{\text{olivine}}$ range extends from normal mantle values (5.0–5.4%; Eiler, 2001; Mattey et al., 1994) to lower values, which are also lower than those previously reported for Payenia (5.02–5.42%; Jacques et al., 2013). Figure 6 demonstrates the relationship between the sampling locations of the Payenia lavas and $\delta^{18}O_{\text{olivine}}$ values: the lowest $\delta^{18}O_{\text{olivine}}$ values in Payenia occur in the Buta Ranquil samples (4.84–5.01%), intermediate $\delta^{18}O_{\text{olivine}}$ values in the Nevado samples (5.23–5.39%). Although the $\delta^{18}O_{\text{olivine}}$ values of VF lavas span a similar range (4.88–5.52%, Jacques et al., 2013), they lack a clear trend in the spatial distribution of $\delta^{18}O_{\text{olivine}}$ variation. VF samples identified by Jacques et al. (2013) as material erupted from isolated satellite cones do not represent endmember $\delta^{18}O_{\text{olivine}}$ values.

4. Discussion

Isotopes and trace element compositions of our samples indicate that the source of the south-central area lavas was less influenced by subduction-related processes than those of Nevado and Buta Ranquil area lavas, consistent with previous reports that identify heterogeneous sources for Payenia (e.g., Jacques et al., 2013; Kay et al., 2013; Søager et al., 2013). Importantly, Payenia lavas do not display a clear link between the strength of the arc geochemical signature and distance from the VF; namely, Nevado lavas have the strongest trace element arc signature and erupted farther away from the VF. The potential causes controlling compositional variability in Payenia lavas are discussed below.

4.1. The Potential Influence of Magma Differentiation and Crustal Contamination on Nevado and South-Central Lavas

Nevado and south-central lavas exhibit clear trends in major and compatible trace element (Ni and Cr) concentrations indicative of olivine \pm clinopyroxene fractional crystallization (Figure 7; e.g., increasing SiO₂, Al₂O₃, TiO₂ K₂O, and Na₂O and slightly decreasing CaO and FeO and initially constant but then decreasing CaO/Al₂O₃ ratios with decreasing MgO, Ni, and Cr). By considering samples within each region that share similar isotopic contents but variable MgO concentrations, we evaluated the extent of crystal fractionation using alphaMELTS (Asimow et al., 2004; Smith & Asimow, 2005). Modeled liquid lines of descent (LLDs) were calculated using high-Mg#, high-Ni Payenia lava compositions as a parent melt for each group at crustal pressures of 3 kbars and initial water contents of 2 wt. % and 0.5 wt.% for the Nevado and south-central sample groups, respectively (Figure 7). Model results reproduce the major element trends defined by the samples. Both LLDs crystallize olivine and then clinopyroxene within the range of MgO concentrations of the samples in this study. Additional LLD modeling details are presented in the Supporting Information S1.

Figure 5. (a) and (b) ⁸⁷Sr/⁸⁶Sr versus ¹⁴³Nd/¹⁴⁴Nd, (c) ¹⁷⁶Hf/¹⁷⁷Hf versus ¹⁴³Nd/¹⁴⁴Nd, (d) and (e) ²⁰⁷Pb/²⁰⁴Pb versus ²⁰⁶Pb/²⁰⁴Pb, and (f) and (g) ²⁰⁸Pb/²⁰⁴Pb versus ²⁰⁶Pb/²⁰⁴Pb. Error bars are 2 σ standard deviation external reproducibility. For Pb isotopes, error bars are smaller than symbol size. Chile Trench sediments are from Lucassen et al. (2010) and Jacques et al. (2013). Nazca metalliferous sediment data from Dekov et al. (2010). EPR MORB data taken from the compilation of Gale et al. (2013). MORB data from the Discovery and Shona segments of the southern Mid-Atlantic Ridge (MAR) taken from Douglass et al. (1999) and Andres et al. (2002). Mesoproterozoic San Rafael Block basement values from (Cingolani, Basei et al., 2017). Mesoproterozoic Andean Precordillera basement values from Kay et al. (1996). Paleozoic to Cenozoic Andean basement (36–41°S) from Lucassen et al. (2004). Symbols and literature sources for VF and Payenia samples are the same as in Figure 2. Northern Hemisphere Reference Line (NHRL, gray dashed line) in the Pb-Pb plots from Hart (1984). The green line representing the mantle array in the Hf-Nd plot from Chauvel et al. (2008).

CHILSON-PARKS ET AL. 10 of 32

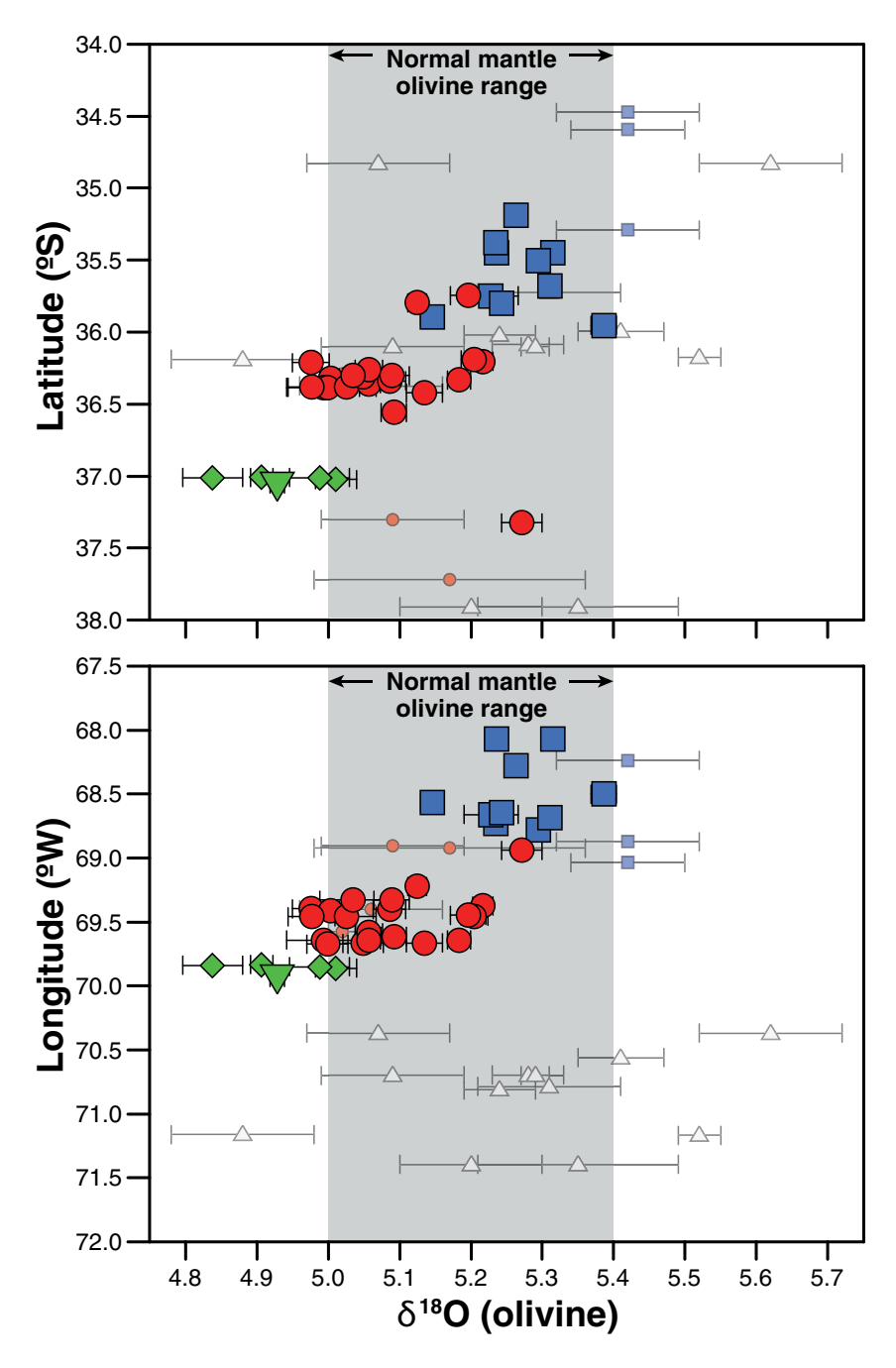


Figure 6. $\delta^{18}O_{olivine}$ values of Payenia and VF lavas versus latitude and longitude of sample localities. Error bars are 1σ standard deviation. Smaller and semi-transparent symbols from Jacques et al. (2013).

Crustal contamination may have played a role in the geochemical variation observed in the Payenia lavas (Søager et al., 2013), but we cannot thoroughly evaluate its importance due to the limited number of Phanerozoic and Proterozoic crustal samples analyzed and the large isotopic variation they define (Abre et al., 2017; Cingolani, Basei, et al., 2017, Cingolani, Llambias, Basei et al., 2017, Cingolani, Llambias, Chemale et al., 2017).

Although we cannot disprove that crustal contamination plays some role in the composition of some Payenia lavas, we can state that crustal contamination is not the main process defining their isotopic variation. We base this assertion on the following findings: (a) The Sr, Nd, and Pb isotopic composition of Mesoproterozoic, Paleozoic, and Mesozoic metamorphic and intrusive rocks do not define an end-member component that can be

CHILSON-PARKS ET AL. 11 of 32



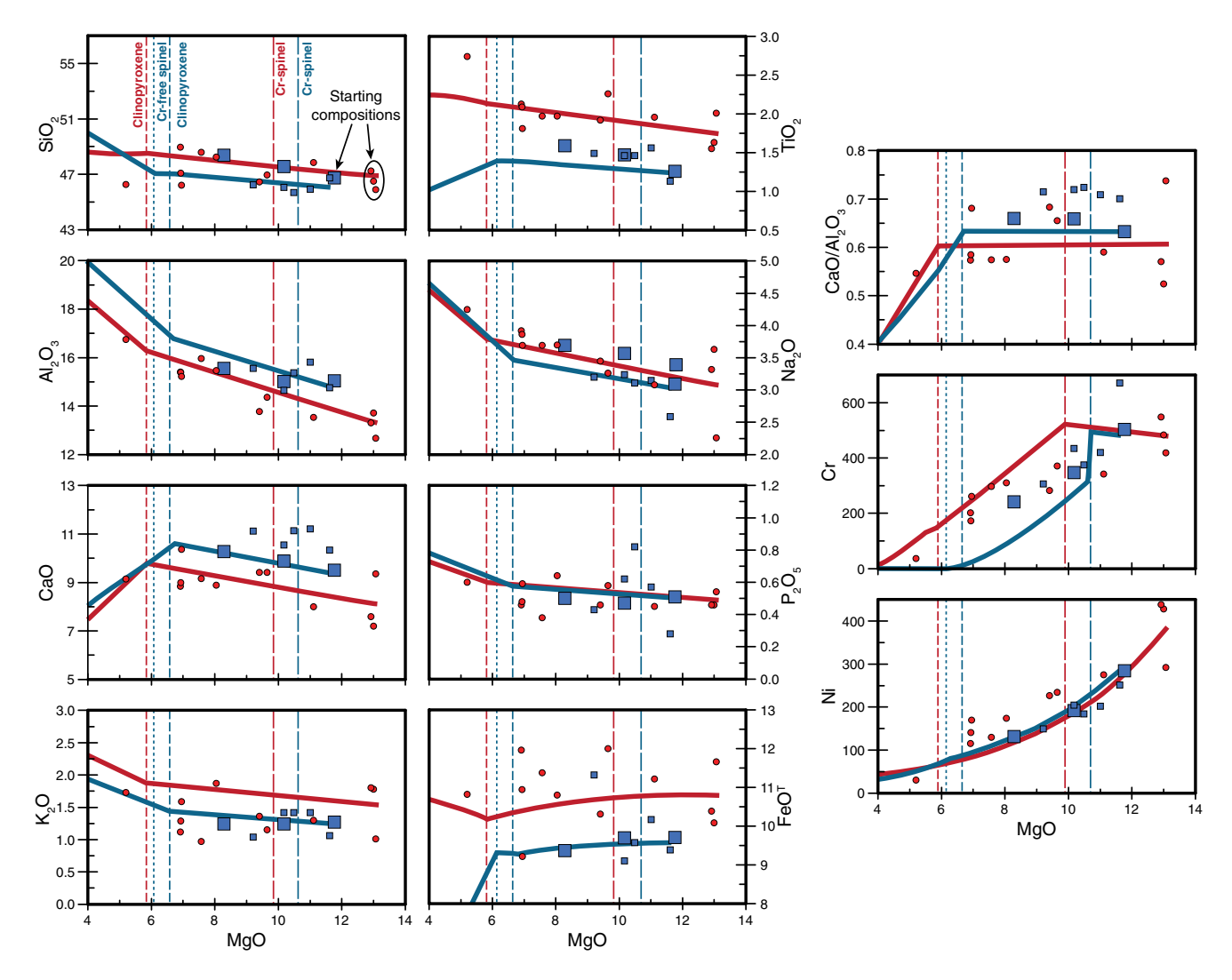


Figure 7. Compositional variations of Payenia lavas compared with modeled liquid lines of descent (LLDs) of primitive Payenia basalts. Bold lines represent the LLDs that were calculated using primitive melt compositions from the Nevado (blue) and south-central (red) areas. Bold red circles and blue squares each represent a subset of samples from the Nevado and south-central areas, respectively, that were chosen due to the similarity of their Pb, Sr, and Nd isotope ratios to those of the samples used as the starting compositions. Faded symbols represent sample compositions reported in this work. Small symbols represent literature data. Note that starting compositions, which are indicated in the SiO₂ versus MgO plot, are slightly offset from LLDs due to the consideration of parent melt H₂O concentration. Dashed lines represent the MgO values at which the stated mineral phases appear along the LLD of the same color. More details about LLD modeling are found in the Supporting Information S1.

responsible for the isotopic variation of the Payenia lavas (Jacques et al., 2013; Figures 5a, 5d, and 5f). (b) Payenia and VF lavas share the same range in Sr and Nd isotopes (Figure 5b) but erupted on different accreted terranes (Ramos, 2009), indicating that the basement did not control the isotopic composition of the lavas (Kay et al., 2013). (c) The variation in Pb isotopes of the Payenia and the VF lavas is delimited by two main components: one at high $^{206}\text{Pb}/^{204}\text{Pb}$, defined by the composition of the trench sediments, and another at low $^{206}\text{Pb}/^{204}\text{Pb}$, which is closer to the composition of the Discovery-Shona MAR MORBs. Both components have Pb isotopes quite different from Mesoproterozoic, Paleozoic, and Mesozoic crustal rocks (Figures 5d and 5f). (d) Most Payenia samples have $\delta^{18}O_{\text{olivine}}$ values within or below the range for normal mantle olivine and have MgO >6 wt.%, indicative of their mantle-derived character.

In accordance with the mantle-derived character of oxygen isotopes of olivine phenocrysts from Payenia lavas, Pb isotopes of potential crustal contaminants do not represent a viable endmember component in the Payenia lava source. Mesoproterozoic crustal rocks beneath Payenia from the San Rafael Block and from the nearby Andean Precordillera have low ¹⁴³Nd/¹⁴⁴Nd and ²⁰⁶Pb/²⁰⁴Pb, ²⁰⁷Pb/²⁰⁴Pb, ²⁰⁸Pb/²⁰⁴Pb, ²⁰⁸Pb/²⁰⁴P

CHILSON-PARKS ET AL. 12 of 32



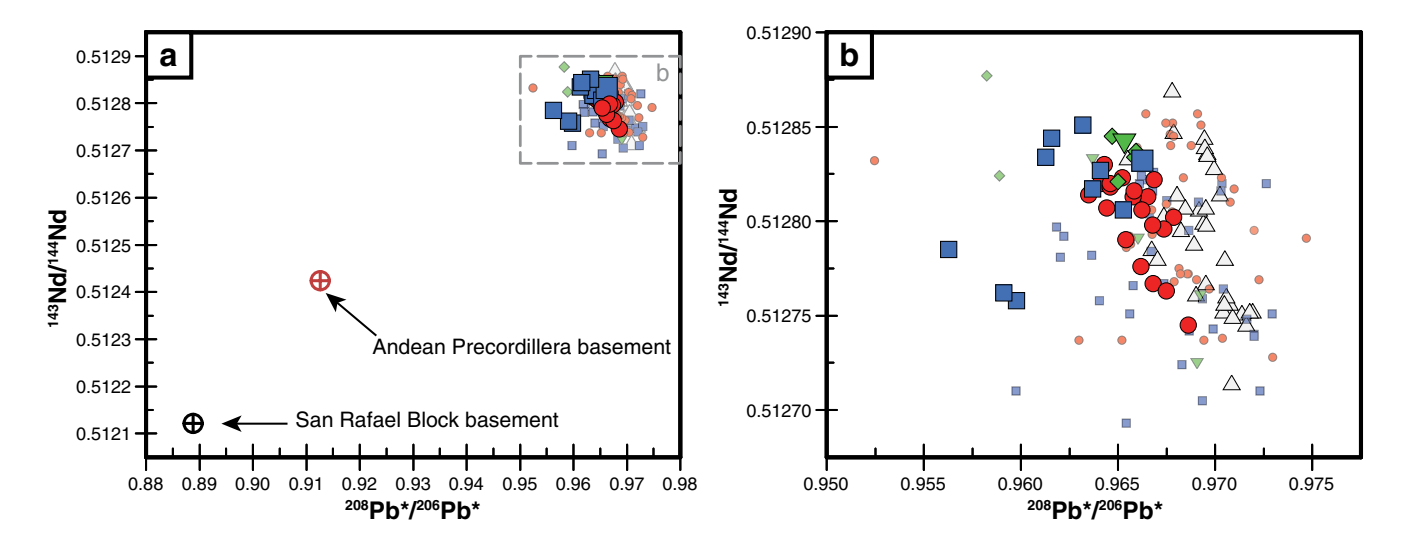


Figure 8. ²⁰⁸Pb*/²⁰⁶Pb* versus ¹⁴³Nd/¹⁴⁴Nd of Payenia and VF samples and concentration-weighted average isotopic composition of the Mesoproterozoic crust of La Ventana Formation in the San Rafael Block (Cingolani, Basei et al., 2017) and Precordilleran basement xenoliths (Kay et al., 1996) Payenia, VF, and Mesoproterozoic crust symbols are the same as in Figure 5. Panel b has the same bounds as the gray dashed box in panel a.

(Figure 8; Cingolani, Basei, et al., 2017; Kay et al., 1996). Therefore, Mesoproterozoic crust could be considered a possible contaminant in some Nevado lavas with low Nd and Pb isotopes. Nevertheless, when we compare the linear trend defined by the Payenia lavas in Pb-Pb isotope diagrams to those of the Mesoproterozoic crustal rocks, the Payenia lavas require a higher Δ7/4 and Δ8/4 endmember than the observed values of the crustal rocks. Moreover, Payenia lavas define an array in ²⁰⁸Pb*/²⁰⁶Pb* versus ¹⁴³Nd/¹⁴⁴Nd that does not trend toward the isotopic composition of Mesoproterozoic crustal samples (Figure 8). Only three Nevado samples (16–4, 16–5, and 19–7) and some literature data plot displaced from the Payenia trend in the direction of the Mesoproterozoic crust. In particular, samples 16–4 and 16–5 are hy-normative and have distinctively high SiO₂, low CaO, K₂O, MgO, and P₂O₅ contents, low Mg#, low ¹⁷⁶Hf/¹⁷⁷Hf, ¹⁴³Nd/¹⁴⁴Nd, Δ8/4, Δ7/4, and high ⁸⁷Sr/⁸⁶Sr isotope values when compared to other Nevado samples. These traits suggest that these two lavas represent the clearest evidence of contamination with crustal material, whereas sample 19-7 has evidence of this contamination on the basis of its isotopic composition. Although more isotope data of the San Rafael Block basement are required to further evaluate the influence of continental crust, current observations indicate that crustal contamination was not the dominant factor controlling the composition of the Payenia lavas.

4.2. Compositional Variations in the Buta Ranquil Region Lavas

Buta Ranquil lavas exhibit distinctive compositional traits, such as a change in major elements from ne-normative, as exhibited by south-central lavas, to hy-normative lavas from the Tromen stratovolcano (Figure 3). These changes are associated with a noticeable increase in LILE/HFSE ratios (arc signature) coupled with an increase in Sr and Pb isotope ratios and a decrease in Nd and Hf isotope ratios (Figures 4b and 5). The $\delta^{18}O_{olivine}$ of all Buta Ranquil samples are the lowest values measured in Payenia lavas, below the normal mantle olivine range. These characteristics signify a distinct petrologic history from other Payenia lavas. Because Buta Ranquil lavas are spatially and compositionally related to the Tromen stratovolcano, we evaluate the potential role that Tromen lavas might have had on the Buta Ranquil lava compositions.

Among Buta Ranquil samples, major element concentrations vary systematically along linear trends between the relatively evolved Tromen hy-normative basaltic trachyandesite sample 27–5 and the more primitive ne-normative Buta Ranquil basalt sample 27–4 (Figures 2 and 3). These two samples also represent the two endmember trace element compositions from this area; the hy-normative endmember has the strongest arc signature, whereas the ne-normative endmember has the weakest arc signature with composition akin to those of basalts from the south-central area (Figure 4b). The compositional variation of the Buta Ranquil volcanic field lavas, especially those that are hy-normative basalt, can be explained by the mixing of 20%–40% of the hy-normative Tromen lava 27–5 with 80%–60% of the ne-normative Buta Ranquil basalt 27–4, respectively (Figure 9a). This clearly

CHILSON-PARKS ET AL. 13 of 32

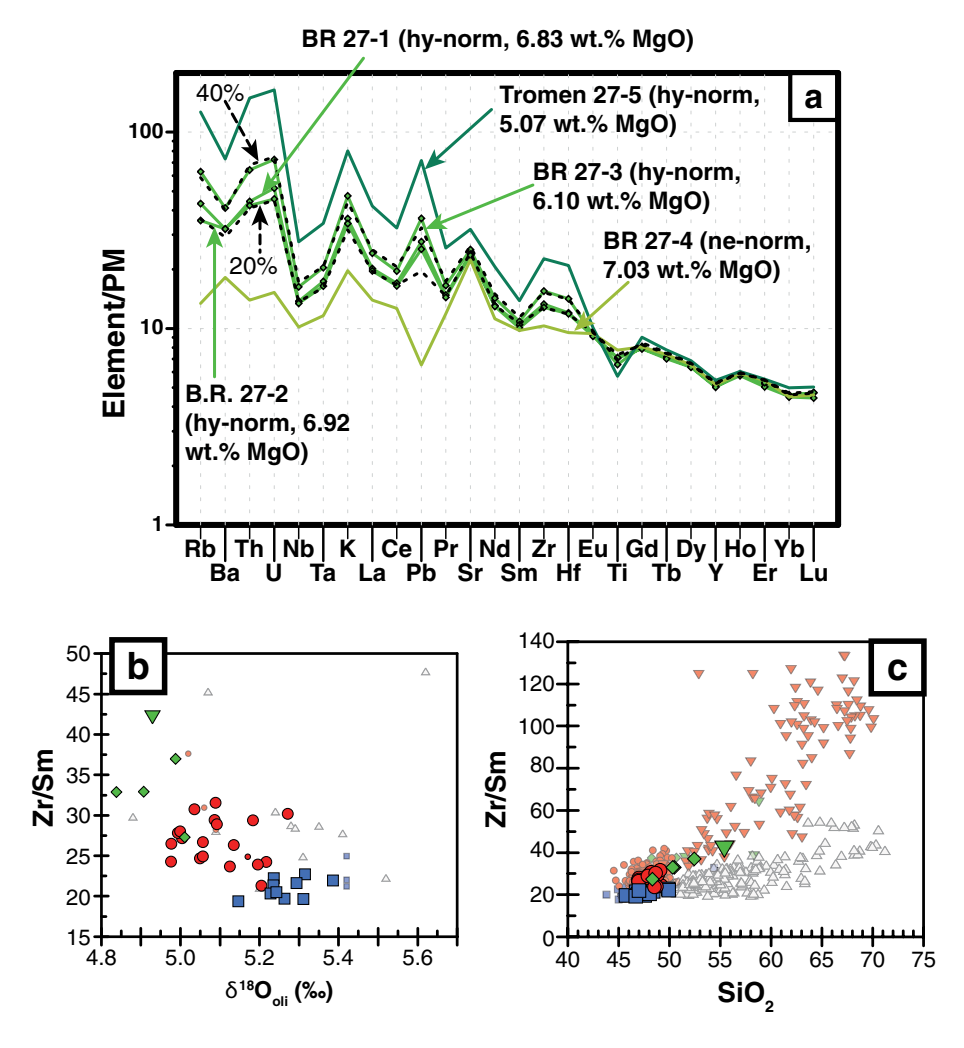


Figure 9. (a) Primitive mantle-normalized trace element diagram showing Buta Ranquil (BR) area lavas compared with mixing calculations between BR sample 27–4 (\sim 1% nepheline normative) and the basaltic trachyandesite sample 27–5 from Tromen (\sim 16% hypersthene normative). Samples 27–1 and 27–2 can be explained as a mixture consisting of 20% hy-norm lava 27%–5% and 80% ne-norm lava 27–4, whereas sample 27–3 requires a 40–60 mixture of these respective components. Primitive mantle values from McDonough and Sun (1995). (b) Zr/Sm versus δ^{18} O_{olivine} and (c) Zr/Sm versus SiO₂. SVZ VF lava compositions from Turner et al. (2016). Red inverted triangles represent evolved (MgO <4 wt.%) lavas from the Payún Liso, Payún Matrú, and Auca Mahuida volcanoes (Espanon et al., 2014; Germa et al., 2010; Hernando et al., 2014; Kay et al., 2013; Pallares et al., 2016; Søager et al., 2013). Other symbols same as in Figure 2.

indicates mixing between lavas from the Tromen stratovolcano with basalts from the associated monogenetic cones of the Buta Ranquil volcanic field.

This mixing trend is also reflected in the radiogenic isotopes of the Buta Ranquil lavas. This is clearly exemplified in Pb-Pb isotope diagrams, where the samples define linear trends with Tromen lava 27-5 having the highest Pb isotope ratios in the area and Buta Ranquil basalt 27-4 the lowest (Figures 5e and 5g). Furthermore, sample 27-4 has Pb isotope values approach those of the ne-normative south-central area lavas. The same is observed, although less well-defined, among Sr, Nd, and Hf isotopes (Figures 5b and 5c).

The low $\delta^{18}O_{\text{olivine}}$ value of the Tromen sample 27-5 seems to control the $\delta^{18}O_{\text{olivine}}$ of the Buta Ranquil hy-normative basalts generated during magma mixing with Buta Ranquil basalt 27–4, which has $\delta^{18}O_{\text{olivine}}$ values within the range of the ne-normative south-central area lavas (Figure 9b). We deem the most likely cause for the low $\delta^{18}O_{\text{olivine}}$ in the Tromen lavas is either progressive, closed-system fractional crystallization, similar to the model presented by Bucholz et al. (2017), or the addition of material that was hydrothermally altered by meteoric waters (e.g., Wang & Eiler, 2008; Watts et al., 2019), or a combination of both processes. Furthermore, low $\delta^{18}O_{\text{olivine}}$

CHILSON-PARKS ET AL. 14 of 32



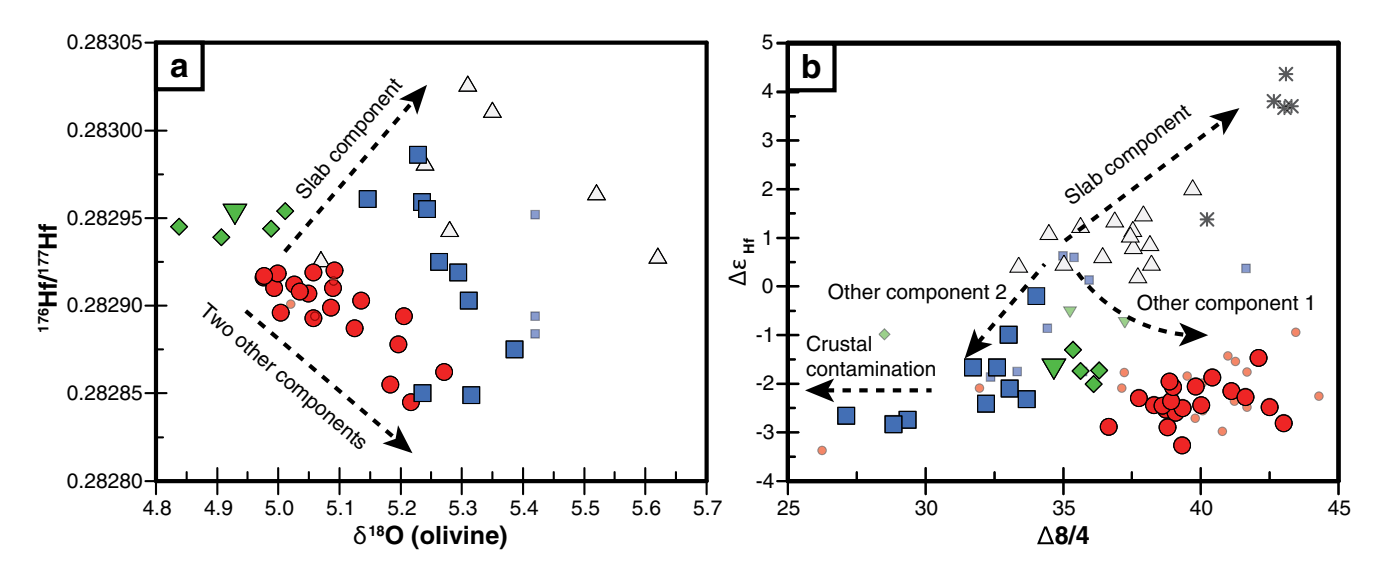


Figure 10. (a) 176 Hf/ 177 Hf vs. δ^{18} O_{olivine} and (b) $\Delta \varepsilon_{Hf}$ versus $\Delta 8/4$ of Payenia and VF lavas and trench sediments. Dashed arrows indicate the inferred causes of the compositional trends discussed in Section 4.3. of the text. Symbols are the same as in Figure 5.

values of Tromen basaltic trachyandesite 27–5 are associated with a high Zr/Sm ratio, quite different from those of the more primitive Payenia lavas (Figure 9b; Zr/Sm = 42, for sample 27–5 vs. Zr/Sm = 19–32 for Nevado and south-central area samples). The covariations in Zr/Sm ratios with SiO₂ contents in Payenia basalts and Payún Matrú, Auca Mahuida, and VF lavas suggest that the effect of magmatic differentiation is responsible for the high Zr/Sm ratios (Figure 9c). This is consistent with fractional crystallization of phases such as amphibole and clinopyroxene ± accessory phases (apatite, titanite, and allanite) with mineral-melt partition coefficients higher for Sm than Zr (Pilet et al., 2011); separation of those phases will increase the Zr/Sm ratio of the residual melt during progressive crystal fractionation. The difference in the Zr/Sm-SiO₂ trend defined by the VF lavas versus the trend defined by samples from the back arc Auca Mahuida and Payun Matru shield volcanoes is likely controlled by the effect of temperature, pressure, and water content of melts undergoing crystal fractionation (Lee & Bachmann, 2014).

In summary, in addition to the clear evidence for mixing in the Buta Ranquil-Tromen magmatic systems, crystal-liquid segregation also appears to be an important process in generating some of the observed major and trace element trends and low $\delta^{18}O_{\text{olivine}}$ observed in lavas from this location. The $\delta^{18}O_{\text{olivine}}$ of the ne-normative Buta Ranquil basalt 27–4 will be evaluated together with the south-central and Nevado lavas in the following section.

4.3. The Geochemical Variability of Nevado and South-Central Lavas

The variation in radiogenic and oxygen isotopes of Payenia and VF lavas demonstrates that neither closed system fractional crystallization nor variable melting extent of a homogeneous source is responsible for the geochemical signatures present in these lavas. The Payenia and VF lavas cover a range in Hf isotopes and $\delta^{18}O_{olivine}$ values that define two perpendicular trends (Figure 10a): one trend extends across the sample areas, with increasing values of $^{176}Hf/^{177}Hf$ and $\delta^{18}O_{olivine}$ from the south-central to the Nevado to the VF, and the other trend occurs within each area, delineated by subparallel arrays in which the lowest $^{176}Hf/^{177}Hf$ have the highest $\delta^{18}O_{olivine}$ values. VF samples appear to form part of both trends, suggesting that the processes acting in the back-arc also affect the VF. Similar but less well-defined trends can be observed between $\delta^{18}O_{olivine}$ and Nd isotope ratios, but Pb and Sr isotopes do not show clear trends with $\delta^{18}O_{olivine}$. Furthermore, Payenia and VF lavas seem to define three different end-members in $\Delta\epsilon_{Hf}$ versus $\Delta 8/4$ (Figure 10b) one having high $\Delta 8/4$ and positive $\Delta\epsilon_{Hf}$ typical of the VF lavas and trench sediments, a second with high $\Delta 8/4$ and negative $\Delta\epsilon_{Hf}$ characteristic of south-central basalts, and a third with relatively low $\Delta 8/4$ and negative $\Delta\epsilon_{Hf}$ representing the Nevado lavas. Note that the three Nevado lavas with possible evidence for crustal interaction plot at distinctly lower $\Delta 8/4$ values than other Nevado samples.

CHILSON-PARKS ET AL. 15 of 32



4.3.1. The Influence of the Slab-Derived Inputs

Nevado and south-central lavas have geochemical characteristics that resemble those of the VF samples, not only in their Sr and Nd isotope ratios (Figure 5b), but also in trace element ratios indicative of slab derived material (fluid/melt), such as high LILE/HFSE ratios and positive Pb and Sr anomalies in primitive mantle-normalized trace element patterns (Figure 4). Nevado area lavas have higher LILE/HFSE ratios than south-central basalts, with a subset of the latter group exhibiting small negative Nb-Ta and Ti anomalies, suggesting that the south-central lava source was influenced by subduction inputs to a much lesser extent than the Nevado lava source. As has been previously argued for back-arc settings of the SVZ, Mexico and the Cascades (Johnson et al., 2009; Rowe et al., 2009; Stern et al., 1990), Payenia basalts may reflect a decrease in the slab flux component and associated extent of mantle melting relative to VF volcanics. However, the Nevado area basalts with a relatively strong arc signature erupted farther east, and thus farther from the VF, than the south-central lavas (Figure 1). This spatial distribution of lavas with arc signature is inconsistent with a decrease of subduction-derived inputs with increasing distance from the trench. Some process other than the simple decrease of slab flux toward the back-arc region may be responsible for the compositional variation of the Nevado and south-central lavas. In addition, VF lavas have higher ¹⁷⁶Hf/¹⁷⁷Hf at similar ¹⁴³Nd/¹⁴⁴Nd values compared to Payenia lavas (Figure 5c). This distinction highlights the important contribution of recycled trench sediments, which has higher ¹⁷⁶Hf/¹⁷⁷Hf values at a given ¹⁴³Nd/¹⁴⁴Nd than the mantle array, to the source of the VF lavas. This is confirmed by the similar Pb isotopes of VF lavas and trench sediments (Figures 5d-5g). Furthermore, Pb isotopes of Payenia lavas indicate that two-component mixing with a continuous decrease in slab-component input from the VF to Nevado to south-central region samples would not work. Pb isotopes of the Nevado and south-central samples define a linear trend from the VF lavas influenced by trench sediments to two other source components that points to different ²⁰⁷Pb/²⁰⁴Pb and ²⁰⁸Pb/²⁰⁴Pb values at similar ²⁰⁶Pb/²⁰⁴Pb (Figures 5e, 5g, and 10b). Therefore, given their compositional variation and spatial distribution, Payenia lavas cannot be simply explained by melting of a homogeneous mantle affected by variable input from the subducting slab.

Direct melting of the subducted oceanic crust is also an unlikely hypothesis because the isotopic composition of the VF and Payenia samples indicates the presence of a more enriched mantle composition than EPR MORB (Figure 5). Furthermore, a combined source of EPR MORB \pm Chile Trench sediments would have higher $^{176} Hf/^{177} Hf$ at similar $^{143} Nd/^{144} Nd$ relative to Payenia basalts (Figure 5c), indicating that this potential source is not responsible for the negative $\Delta\epsilon_{Hf}$ values of Payenia lavas. Melts of subducted sediments and/or the upper oceanic crust would also be expected to inherit an enrichment in $^{18} O$ relative to normal mantle (Gregory & Taylor, 1981), but Payenia lavas have $\delta^{18} O_{\text{olivine}}$ values within or lower than mantle values. Therefore, melts of the subducted Nazca slab and/or overlying sediment are not expected to be the direct source of the Payenia lava compositions.

4.3.2. Compositional Heterogeneity in the Sub-Payenia Mantle: Asthenospheric Versus Lithospheric Sources

The observed isotopic and trace element systematics of the south-central, Nevado, and VF lavas reveal the changes in the source composition from the Payenia area to the VF region. This change is characterized by a progressive increase in $\delta^{18}O_{olivine}$, $\Delta\epsilon_{Hf}$ (i.e., $^{177}Hf/^{176}Hf$ controlling the $\Delta\epsilon_{Hf}$), $^{206}Pb/^{204}Pb$, $^{207}Pb/^{204}Pb$, $^{208}Pb/^{204}Pb$, and trace element indicators of arc signature (LILE/HFSE) from the south-central area to the Nevado area to the VF (Figure 10). The large compositional variability in the VF lavas, overlapping with the range in $\delta^{18}O_{olivine}$, $^{143}Nd/^{144}Nd$ and $^{87}Sr/^{86}Sr$ of Payenia basalts (Figures 5b and 6), is a sign that the processes acting in the back-arc also occur in the VF. A second-order trend is observed within each area: among each group of VF, Nevado, and south-central lavas, $^{143}Nd/^{144}Nd$, $^{177}Hf/^{176}Hf$, and $\Delta\epsilon_{Hf}$ exhibit a weak correlation with $\delta^{18}O_{olivine}$, suggesting that at least one source component, present in the VF and Payenia, has relatively high $\delta^{18}O_{olivine}$ and low radiogenic Nd and Hf and low $\Delta\epsilon_{Hf}$ (Figure 10).

The geochemical variations observed in the VF, Nevado, and south-central lavas imply at least three compositional end-members: one having trace element ratios with very strong arc signature (e.g., high Ba/Nb, U/Nb, Pb/Ce), intermediate to high $\delta^{18}O_{olivine}$ and $\Delta 8/4$, and $\Delta \epsilon_{Hf} \geq 0$, which are characteristics of the VF lavas; a second with trace element ratios with minimal to no arc signature, low $\delta^{18}O_{olivine}$ values, negative $\Delta \epsilon_{Hf}$, and high $\Delta 8/4$, which are characteristics of south-central basalts; and a third with intermediate arc trace element signature and $\delta^{18}O_{olivine}$ values, negative $\Delta \epsilon_{Hf}$ and low $\Delta 8/4$, which are characteristics of the Nevado lavas (Figures 10 and 11). The first component represents an asthenospheric source that was partially affected by slab-derived inputs (recycled

CHILSON-PARKS ET AL. 16 of 32



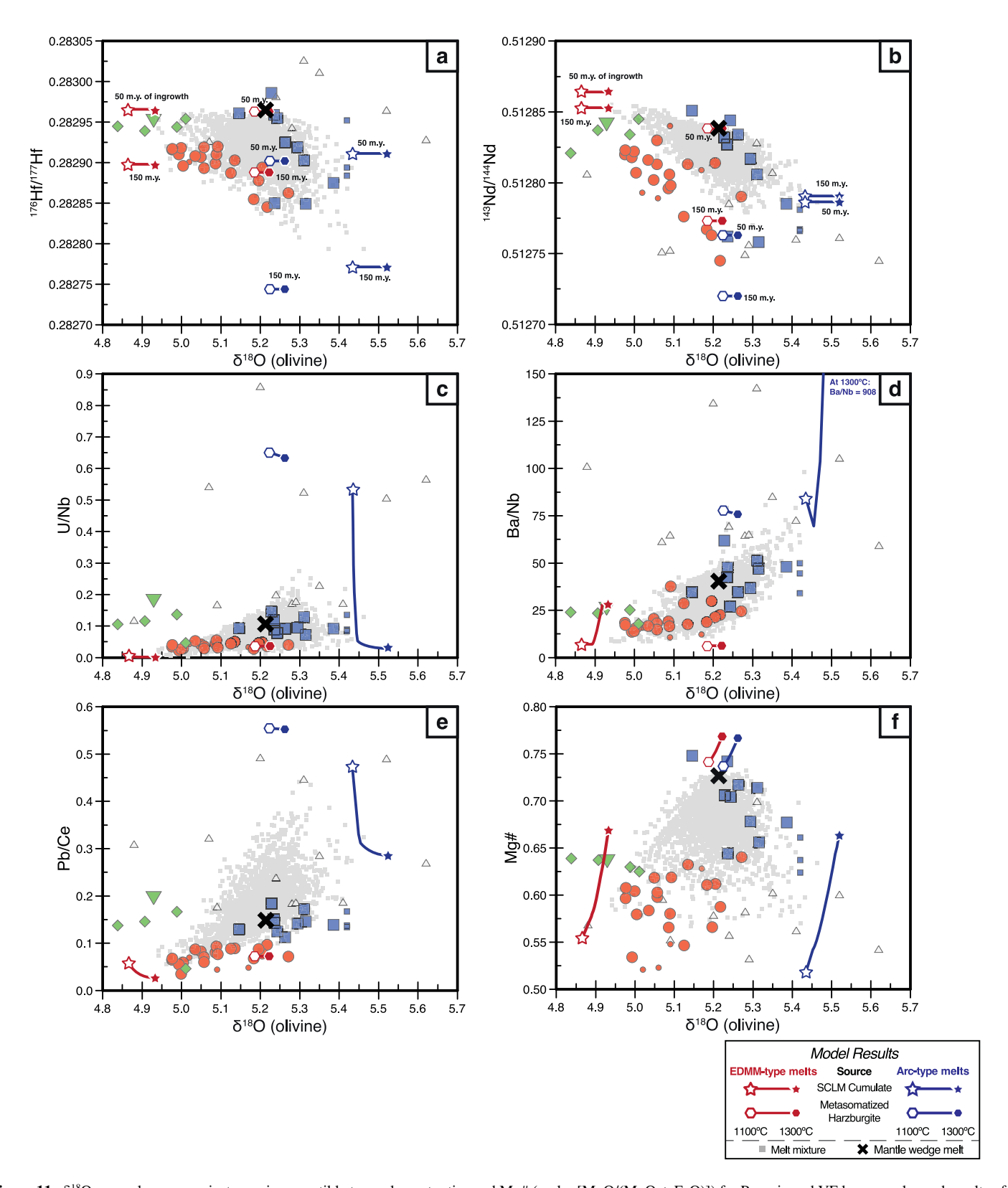


Figure 11. $\delta^{18}O_{\text{olivine}}$ values versus isotopes, incompatible trace element ratios and Mg# (molar [MgO/(MgO + FeO)]) for Payenia and VF lava samples and results of the modeled melt compositions. Red lines represent modeled melt compositions from EDMM-type metasomatized SCLM and blue lines represent melts from arc-type metasomatized SCLM. Lines bounded by hexagons and those bounded by stars represent melts of SCLM cumulate and metasomatized harzburgite, respectively. Empty stars and hexagons represent melt compositions at 1100°C and filled stars and hexagons are melt compositions at 1300°C. Gray squares represent the modeled melt mixtures between SCLM melts, and the black X represents the mantle wedge melt composition. Other symbols same as in Figure 2.

CHILSON-PARKS ET AL. 17 of 32



sediments and fluids). In contrast, the other two source components, with their negative $\Delta \epsilon_{Hf}$ and variable (high and low) $\Delta 8/4$ values, cannot be easily explained by heterogeneities in the asthenosphere.

Previous studies argue that the south-central lavas exhibit trace element and radiogenic isotopes akin to EM-1 type ocean island basalts (i.e., Discovery- and Shona-influenced MAR MORB; Dyhr, Holm, & Llambías, 2013; Dyhr, Holm, Llambías, et al., 2013; Jacques et al., 2013; Kay & Copeland, 2006; Kay et al., 2013; Søager & Holm, 2013; Søager et al., 2013), where the EM-1 source constitutes a peridotite-pyroxenite mixture of ascending asthenospheric mantle (Søager & Holm, 2013; Søager, Portnyagin et al., 2015). However, Hf and Nd isotopes (Figure 5b) and trace element ratio systematics (Figures 12a–12c) reveal that the south-central lava compositions diverge from those of the EM-1 basalts, as well as from all other endmember MORB and OIB compositions. The south-central lavas display trace element ratio variations in Figure 12 that are not expected to result from varying degrees of melting, because each ratio pairs trace elements that partition similarly during mantle melting. Additionally, neither slab-derived nor continental crust-derived inputs would account for the compositions of the south-central lavas.

In contrast, the trace element compositions of silicate glasses in peridotite xenoliths from Patagonia (Aliani et al., 2009; Laurora et al., 2001; Scambelluri et al., 2009), in particular the high-Ti melt pockets and veins reported by Laurora et al. (2001), have distinctively high Ba/Th, K/La, and low U/Nb ratios (Figures 12a and 12b). Therefore, they represent a viable endmember in the trends displayed by south-central lavas and suggest that the metasomatized SCLM played an important role in the generation of Payenia and possibly VF melts, as has been previously proposed to explain the trace element and isotopic compositions of small eruptive centers adjacent to the Villarica volcano in the central SVZ (Hickey-Vargas, Sun, & Holbik, 2016).

Metasomatic enrichment of the SCLM can be caused by low-degree asthenospheric melts, affected or not by subduction processes, which percolate through the SCLM and may precipitate veins of cumulates consisting of anhydrous (e.g., clinopyroxene, garnet, and olivine) and hydrous (e.g., amphibole, phlogopite) mineral phases (Foley, 1992) or may react with the SCLM peridotites to produce pyroxenites (Kilian & Stern, 2002; Pilet et al., 2011; Wang et al., 2008 and references therein). Alkaline basalts from Patagonia bear modally metasomatized mantle xenoliths containing amphibole, phlogopite, and apatite (Aliani et al., 2009; Bjerg et al., 2005; Kilian & Stern, 2002; Laurora et al., 2001; Scambelluri et al., 2009; Stern et al., 1999; Wang et al., 2008). The presence of a phlogopite (+/-amphibole)-bearing veined cumulate melt was also proposed by Søager et al. (2018) for the Payenia lavas based on major and trace element compositions of olivine-hosted melt inclusions. Modeling and experimental studies have shown that the melting of veined cumulates yields major and trace element compositions resembling alkaline lavas from oceanic and continental settings (Condamine & Médard, 2014; Pilet et al., 2008, 2011; Sorbadere et al., 2013).

In light of our observations, we test the possibility that the Nevado and south-central lava compositions can be accounted for by the contribution of two endmembers sourced in the SCLM: one representing SCLM that interacted with a subduction-related parent melt (an "arc-type" component) typical of the Nevado area lavas and another representing SCLM that interacted with a parent melt from ambient upwelling asthenosphere (a trace element enriched MORB mantle source with isotopes equivalent to those of the Discovery- and Shona-type basalts). Because the Payenia melts have Hf and Nd isotopes and trace elements ratios that differ from the VF-, Discovery- and Shona-type basalts (Figures 5c and 12a-12c), Payenia melts were not derived directly from a Discovery- and Shona-type mantle variably affected by slab derived fluid/melt. We propose that the lavas were partially derived from the lithospheric mantle metasomatized by "arc-type" and "EDMM-type" basalts some time before the present (e.g., 100 ± 50 Ma). In the following sections, we describe and discuss a forward model calculation that simulates the melting of a metasomatized SCLM, their mixing with mantle wedge melts, and their compositional resemblance to Payenia lavas.

4.4. Modeling SCLM Metasomatism With Cumulate Formation and Subsequent Melting

We test the hypothesis that Nevado and south-central lavas represent mixing of melts originating from the mantle wedge and the metasomatized SCLM beneath Payenia (Figure 13). Our forward model is consistent with Payenia lava compositions resulting from the melting of cumulates and metasomatized harzburgite in the SCLM and subsequent mixing of these melts with asthenospheric mantle wedge melt. Given the lack of correlation between a

CHILSON-PARKS ET AL. 18 of 32



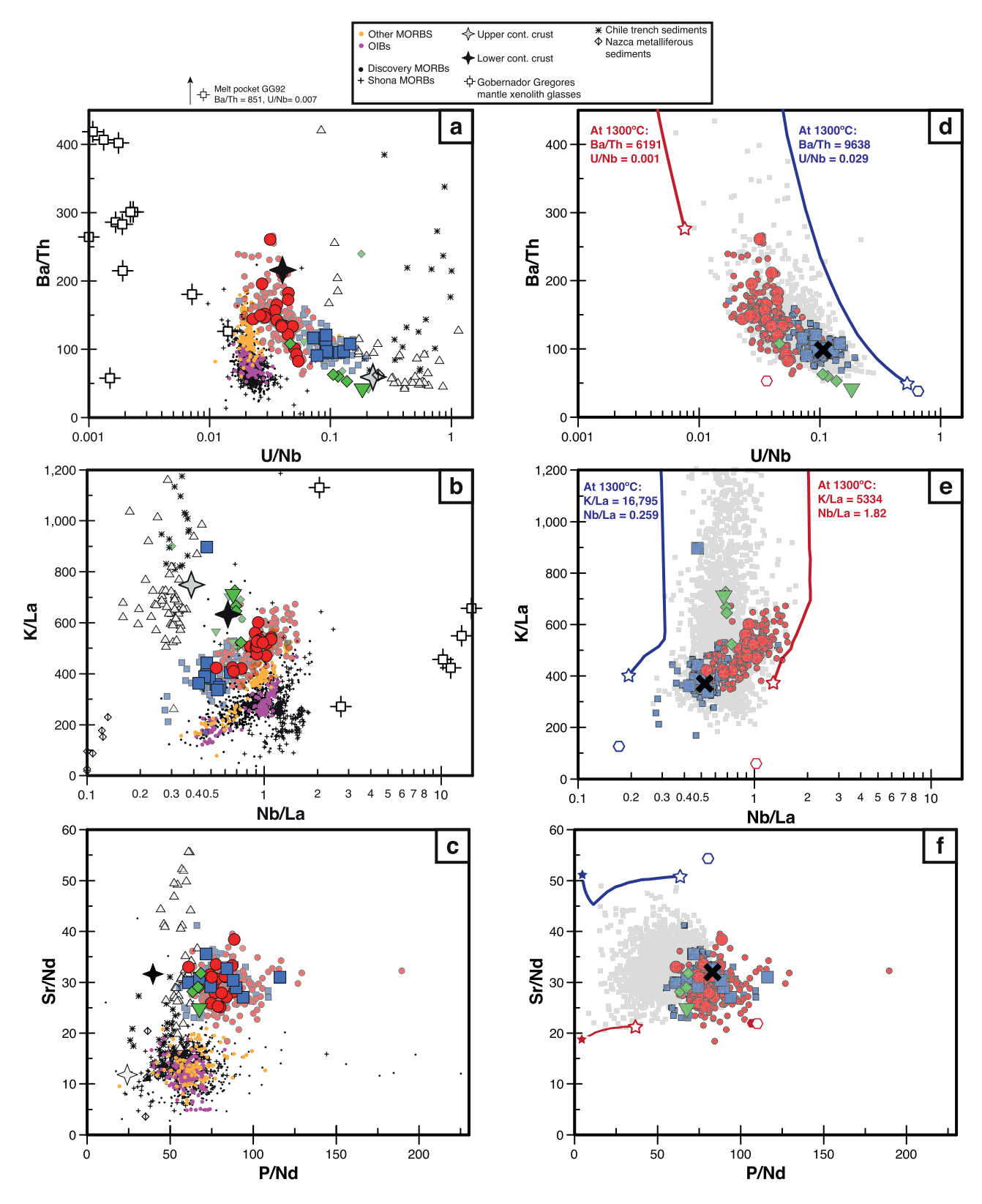


Figure 12.

CHILSON-PARKS ET AL. 19 of 32

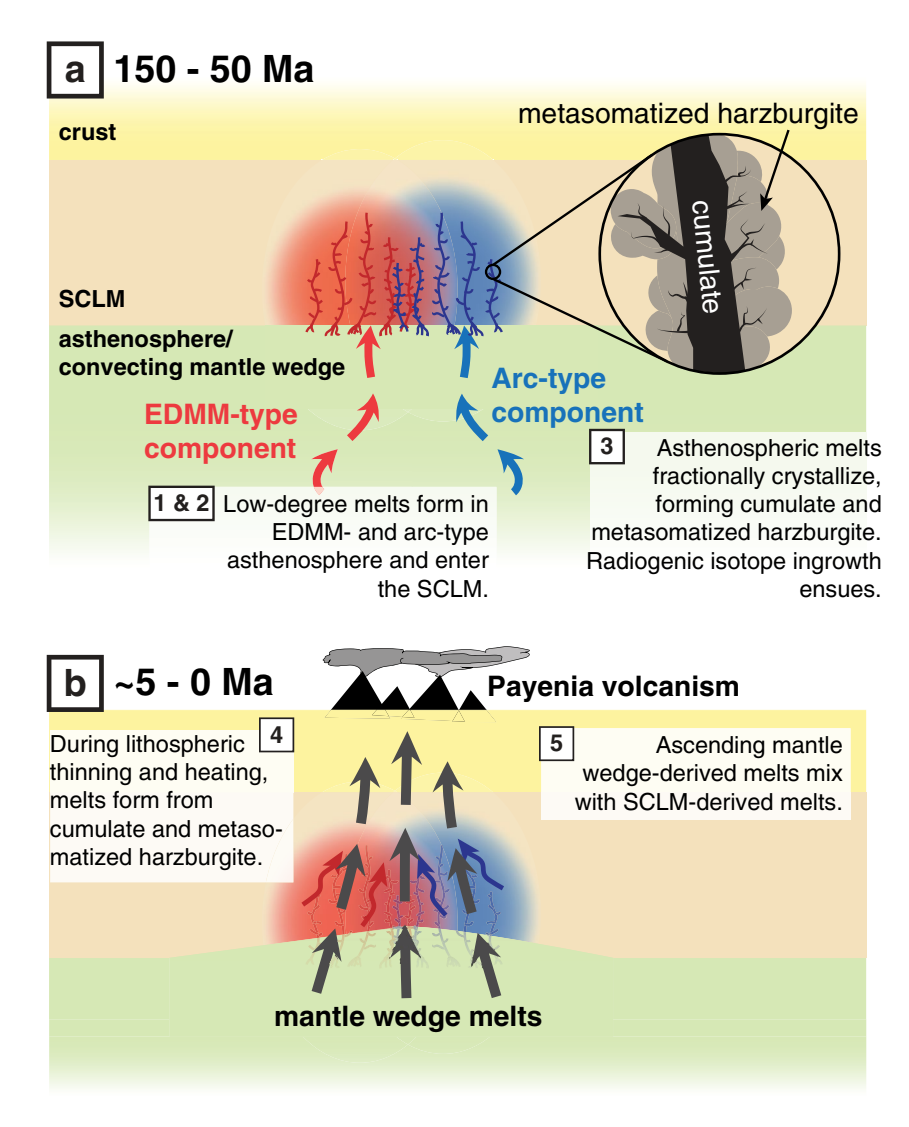


Figure 13. Cartoon conceptualization of the forward model presented in this study. Numbered steps same as in Table 1. Figure modified from Pilet et al. (2011).

decrease in arc signature and distance to the VF for the Payenia lavas, we assume two different types of cumulate compositions in the SCLM: one type was influenced by asthenospheric melts generated from an EDMM source (Discovery-Shona MORB source), which is more closely associated with the south-central lavas, and another that was influenced by melts generated from the mantle-wedge during subduction zone processes, which is more closely associated with the Nevado lavas.

Model steps and parameters are detailed in Table 1 and Figure 13.

Figure 12. Relations between incompatible trace elements Ba/Th versus U/Nb, K/La versus Nb/La, and Sr/Nd versus P/Nd for VF and Payenia samples with MgO >5 wt.%. The left column of plots compare Payenia lava compositions with average compositions of upper and lower continental crust (Rudnick & Gao, 2014), VF lavas, Chile Trench sediments, Nazca Plate metalliferous sediments, Discovery- and Shona-type MORBs (compiled from PetDB), other MORBs and OIBs (also from PetDB), and glasses from Patagonian peridotite xenoliths (Aliani et al., 2009; Laurora et al., 2001; Scambelluri et al., 2009). Symbols and lines for model results same as in Figure 11. Note that xenolith glass data is lacking for Sr/Nd versus P/Nd, and that in panels d, e, and f, most modeled melts of metasomatized harzburgite exhibit compositional variations smaller than the size of the corresponding symbol.

CHILSON-PARKS ET AL. 20 of 32



Table 1		
Step no.	f Model Inputs and Procedures Step description	Step details
0	General model details	All simulations of melting and crystallization were performed in pHMELTS, using the alphaMELTS interface.
		 All mineral-melt partition coefficients were from previous estimates for phases typically involved in mantle melting and melt crystallization.
		 All calculations of oxygen isotope fractionation between melt and mineral phases were performed based on a previously published approach.^c
1	Starting composition of EDMM- and arc-type asthenospheric mantle sources	 Major element concentrations for both types of mantle sources were from previous estimates of DMM.^d
		 For the EDMM-type asthenosphere, trace element concentrations were taken from previous estimates.^c The H₂O concentration for EDMM-type asthenosphere are based on previous estimates of EDMM water contents.^f Radiogenic isotopes are representative values for Discovery-Shona MAR MORBs.^g
		• For the arc-type asthenosphere, trace element concentrations were calculated using the composition of a primitive (Mg# = 0.70) alkaline lava sample CL196 with strong arc trace element signature, which erupted from a small cone near the Cerro Azul stratovolcano in the VF. ^h We derived its mantle source composition assuming the sample represents 5% batch melting of a garnet peridotite. The assumed H ₂ O concentration of 1,500 ppm for the mantle wedge is based on previous estimates of SVZ mantle wedge H ₂ O contents. ^j Radiogenic isotopes of the arc-type asthenosphere are representative values for VF lavas. ^j
2	Generation of asthenospheric melt	 Melts generated from both asthenospheric mantles (affected and not affected by subduction) produced metasomatism SCLM that was assumed to occur 50–150 Ma.
		• EDMM-type asthenosphere melting was modeled isobarically (at 2.5 GPa) up to $F = 1\%$ before entering the SCLM, consistent with a low-degree melt metasomatizing agent. The δ^{18} O of the melt was assumed to be 5.7%, a value in equilibrium with normal mantle olivine.
		• Arc-type asthenosphere melting was modeled isobarically (at 2.5 GPa) up to $F = 3\%$ before entering the SCLM. The δ^{18} O of the melt is assumed to be 6.2 ‰, an average value for mafic SVZ lavas. ^m
3	Formation of crystal cumulates and metasomatized harzburgite in the SCLM	• Fractional crystallization of both types of asthenospheric melts were calculated under isobaric conditions at $P = 1.5$ GPa and until $T = 900$ °C, reflective of the equilibration pressures and temperatures recorded by nearby mantle xenoliths.
		• The residual melt that remained after the formation of the mafic cumulates was assumed to interact with a trace element-free harzburgite (20% orthopyroxene, 80% olivine). These compositions were mixed in a 95:5 ratio of harzburgite to residual melt, producing the composition and mineralogy of the modeled metasomatized harzburgite in alphaMELTS.
		• Rb, Sr, Sm, Nd, Lu, Hf, U, Th, and Pb concentrations of the mafic SCLM cumulates and metasomatized harzburgite are used to estimate their present-day isotope values given that isotopic ingrowth would have started at 50–150 Ma.
4	Melting of cumulates and harzburgite	 Melting of the EDMM-type and arc-type metasomatized SCLM is considered in two different lithologies: the mafic cumulate and the metasomatized harzburgite. The model assumes for both lithologies that melting occurs isobarically at 1.5 GPa within a temperature range of 1100°-1300°C, an approximation of the temperature range previously constrained by compositions of olivine-hosted melt inclusions from Payenia.°
5	Mixing of melt from present day mantle wedge and metasomatized SCLM	• To approximate the composition of the melt from the present-day mantle wedge beneath Payenia we averaged the composition of four Nevado lavas with the highest Mg# $(0.70–0.75)$ and $\Delta\epsilon_{Hf}$ closest to 0.
		 The different melts are mixed in 2000 randomized combinations. For each of these iterations, mixing occurs in three steps:
		i The duration of isotopic ingrowth of Pb, Sr, Nd, and Hf isotopes in the crystal cumulate and metasomatized harzburgite of EDMM- and arc-type metasomatized SCLM was randomly selected between 50 and 150 m.y. The resultant isotopes of these SCLM sources became the values for the melts used in the subsequent mixing calculations.

CHILSON-PARKS ET AL. 21 of 32



Table 1 Continued		
Step no.	Step description	Step details
		ii Randomly determined proportions of cumulate-derived melt and metasomatized harzburgite- derived melt were mixed within the modeled EDMM-type SCLM, and the same was done for the arc-type SCLM. The only constraint in this mixing calculation was that melts of metasomatized harzburgite represent no more than 80% of this mixture.
		iii The two hybrid melts from each SCLM member and the mantle-wedge-derived melt were then mixed in randomly determined proportions.
^a Asimow et al. (2004); Smith and Asimow (2005). ^b Pilet et al. (2011). ^c Bucholz et al. (2017); see Supporting Information S1. ^d Workman and Hart (2005). ^c Workman and Hart (2005). ^c Andreas et al. (2002). Developes et al. (2002). ^c Andreas et		

^aAsimow et al. (2004); Smith and Asimow (2005). ^bPilet et al. (2011). ^cBucholz et al. (2017); see Supporting Information S1. ^dWorkman and Hart (2005). ^eWorkman and Hart (2005) and Salters and Stracke (2004). ^fDixon et al. (2002); Shimizu et al. (2016). ^gAndres et al. (2002); Douglass et al. (1999). ^hJacques et al. (2013). ^hWeller and Stern (2018). ^jSee VF references mentioned in the caption of Figure 2. ^kPilet et al. (2011). ^hEiler (2001); Mattey et al. (1994). ^mHickey-Vargas, Holbik, et al. (2016). ⁿBertotto et al. (2013). ^oSøager, Portnyagin et al. (2015).

4.4.1. Model Results

Modeled compositions of the arc- and EDMM-type asthenosphere sources, metasomatic melts, metasomatized SCLM by vein cumulate and residual melt, as well as melts from the mantle wedge, SCLM cumulates, and metasomatized harzburgite are presented in Table S2. The mineral assemblage of the cumulate formed in the lithosphere consisted of 38 wt.% olivine, 35% clinopyroxene, 18% hornblende, 8% phlogopite, and 1% spinel for the EDMM-type melt and of 31% olivine, 40% clinopyroxene, 10% hornblende, 18% phlogopite, and 1% spinel for the arc-type melt.

Modeled major element contents are compared to Payenia lava compositions in Figure 14. Melt mixture concentrations match those of the Payenia lavas except for the CaO and Na₂O (Figure 14), for which the model produced relatively high and low concentrations, respectively. This discrepancy is most likely attributed to the limited compositional variability of amphibole and biotite when they occur as melting and crystallizing phases in alphaMELTS. Major element systematics of the Payenia lavas and modeled melt mixtures also resemble results from experimental studies of mafic cumulates, which represent cumulate assemblages of olivine, clinopyroxene, and amphibole that were mixed with peridotite and melted at 1 GPa (Sorbadere et al., 2013). We also note that the modeled melts derived from metasomatized harzburgite and cumulates have SiO₂ concentrations higher and lower than values for Payenia lavas, respectively (Figure 14). The SiO₂-rich nature of harzburgite-derived melts and the SiO₂-poor nature of the modeled and experimental melts derived solely from SCLM cumulate is consistent with the observation that intraplate alkali magmas range in composition from silica-undersaturated nephelinites to alkali basalts. Silica enrichment by ~4–5 wt.% has been demonstrated by melts experimentally produced from a hornblendite-peridotite sandwich experiments versus melts from a hornblendite-only source (Pilet et al., 2008).

The modeled cumulate-derived melts have Mg# = 0.52–0.67, which covers the lowest Mg# values of Payenia lavas, whereas the metasomatized-harzburgite-derived melts have Mg# = 0.74–0.77, a range that exceeds that of Payenia Mg# values (Figures 11f). Furthermore, the highest and lowest Payenia $\delta^{18}O_{olivine}$ values closely resemble values from the EDMM-type and arc-type cumulate-derived melts, respectively, whereas both types of the metasomatized-harzburgite-derived melts have $\delta^{18}O_{olivine}$ values close to the mantle average of 5.2‰. These covariations in Mg# and $\delta^{18}O_{olivine}$ of the modeled melts reproduce the trends displayed by Payenia lavas for these parameters.

Trace element concentrations and patterns in primitive mantle normalized and isotope ratios of the modeled melt mixtures resemble those of south-central and Nevado samples (Figures 11, 12, 15, and 16). The modeled melts from the EDMM-metasomatized SCLM reproduce the distinctive trace element patterns, low radiogenic Pb, 176 Hf/ 177 Hf, and δ^{18} O_{olivine} values exhibited by south-central lavas, whereas the melts from Arc-metasomatized SCLM melts reproduce the trace element arc signature, the δ^{18} O_{olivine} values and the low 176 Hf/ 177 Hf values exhibited by the Nevado lavas. Additionally, the trace element characteristics of melts from EDMM-metasomatized SCLM resemble those of Patagonian melt pockets in their high Ba/Th, K/La, Nb/La, Sr/Nd,

CHILSON-PARKS ET AL. 22 of 32



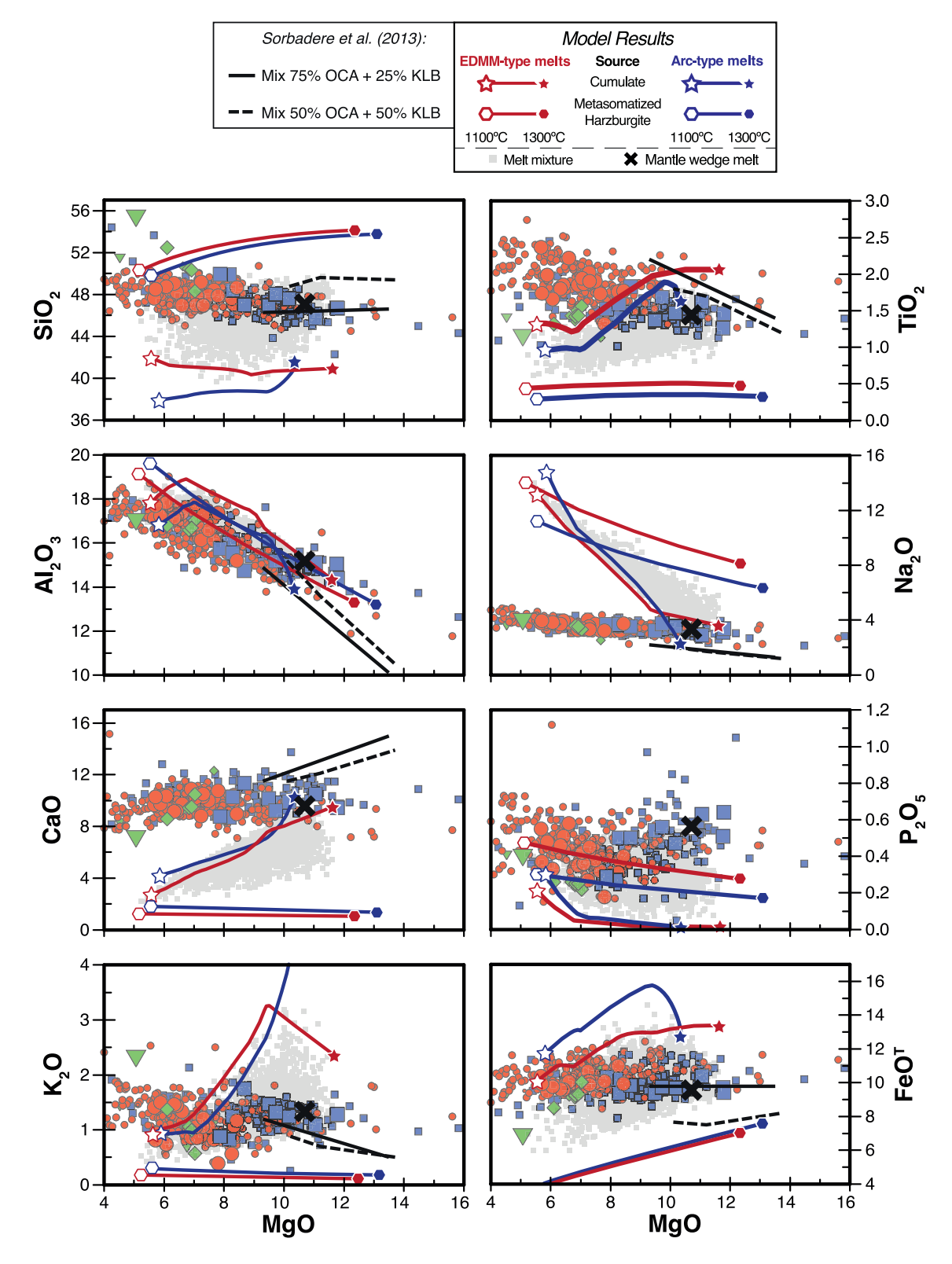


Figure 14. Major element concentrations of modeled melts compared with Payenia samples. Sample and model symbols same as in Figure 11. Black lines represent experimental glass compositions reported by Sorbadere et al. (2013), which were generated from melting mixtures of OCA (olivine-amphibole clinopyroxenite) KLB-1 (peridotite) at 1 GPa in proportions of 50% OCA and 50% KLB-1 (solid lines) and 75% OCA and 25% KLB-1 (dashed lines).

CHILSON-PARKS ET AL. 23 of 32



P/Nd, and low U/Nb (Figures 12d–12f), which demonstrates that the geochemical signature of Payenia lavas was largely inherited from a metasomatized SCLM source similar in composition to the Patagonian xenoliths melt pockets. The negative Pb anomalies seen in some south-central lava trace element patterns are not consistently reproduced by the modeled lavas (Figure 15b). This discrepancy may be because sulfides, which are present in SCLM xenoliths and would be enriched in Pb, were not included as a potential phase in the modeling calculations.

Melts from EDMM-metasomatized SCLM reproduce the relatively low $\delta^{18}O_{olivine}$ values of south-central lavas because of mineral-melt oxygen isotope fractionation. This effect has been overlooked as a potential mechanism for lowering the $\delta^{18}O_{olivine}$ values of basaltic magmas. Instead, previous studies have attributed low- $\delta^{18}O_{olivine}$ values measured in subduction-related basalts to the contribution of low- δ^{18} O fluids released from the deep portions of the subducting slab that underwent high-temperature (>350°C) hydrothermal alteration prior to subduction (Eiler et al., 2005; Martin et al., 2011). While this hypothesis may explain the low $\delta^{18}O_{olivine}$ values we measured, our model does not rely on inputs from the subducting slab to yield $\delta^{18}O_{olivine}$ values as low as ~4.9%. In our model calculations, the fractionation factors of oxygen isotopes between the clinopyroxene and amphibole forming the vein-cumulate and asthenospheric melt are both about -0.6%, as averaged across the temperature range of the modeled SCLM metasomatism. Mineral-melt fractionation factors during both crystallization and melting are determined using the temperature, melt fraction, mineral assemblage, and melt composition outputs from alphaMELTS. When clinopyroxene and amphibole melt, they impart lower δ^{18} O values to the melts. Our model demonstrates that the mineral phases involved in the metasomatism of the SCLM during veined cumulate formation can significantly influence the oxygen isotopes of the mafic melts generated during melting of the metasomatized SCLM, even though the melt responsible for the metasomatism had oxygen isotopes within the normal range of the MORB source.

The radiogenic isotope ingrowth trends of EDMM- and arc-type metasomatized SCLM show that an isotopic ingrowth duration of 50–150 m.y. matches or exceeds the most negative $\Delta \epsilon_{Hf}$ values of Payenia lavas (Figure 16, Table S3). These results suggest that the dominant period of metasomatism in the SCLM source of the Payenia lavas occurred at 50–150 Ma.

We acknowledge that these results represent a simplification of the generation and evolution of SCLM-derived melts. Nonetheless, the mineral assemblages of cumulates from both endmembers resemble those determined from geochemical modeling, experiments, and petrological observations of lithospheric veined cumulates (Pilet et al., 2011 and references therein).

4.4.2. Implications of Model Results

When considering causes for the melting of the SCLM responsible for the Payenia lava compositions, the simplest explanation involves tectonic extension, lithospheric thinning, and heating from upwelling asthenosphere. A likely cause for this process is the inflow of hot asthenosphere beneath Payenia during the Pliocene-Quaternary episode of slab steepening and regional extension (Kay, Burns, et al., 2006; Ramos & Folguera, 2011). Geophysical observations show that in the present-day mantle beneath Payenia, an anomalous low seismic velocity and high electrical conductivity currently occupies the shallow asthenosphere (Burd et al., 2014; Gilbert et al., 2006), which may signify a thermal anomaly responsible for the heating and melting of the SCLM.

We must also address the 50–150 million years of isotopic ingrowth needed to reproduce the trends in the radiogenic isotopes of the Payenia lavas. This period follows the ~180 Ma initiation of the breakup of the Gondwana supercontinent, at which time South America rifted from Africa, opening the South Atlantic Ocean (Franzese et al., 2003; Ramos, 1999, 2005). During the same period, along the western margin of South America, subduction of the proto-Pacific plate had initiated arc magmatism (Gordon & Ort, 1993; Haller & Lapido, 1980; Lizuain, 1999). These two tectonic events would generate mantle melts associated with both rifting-related adiabatic decompression and subduction processes. The compositional variation expected from this variety of mantle melts agrees with the occurrence of the arc-type and EDMM-type metasomatic agents in the model presented.

CHILSON-PARKS ET AL. 24 of 32



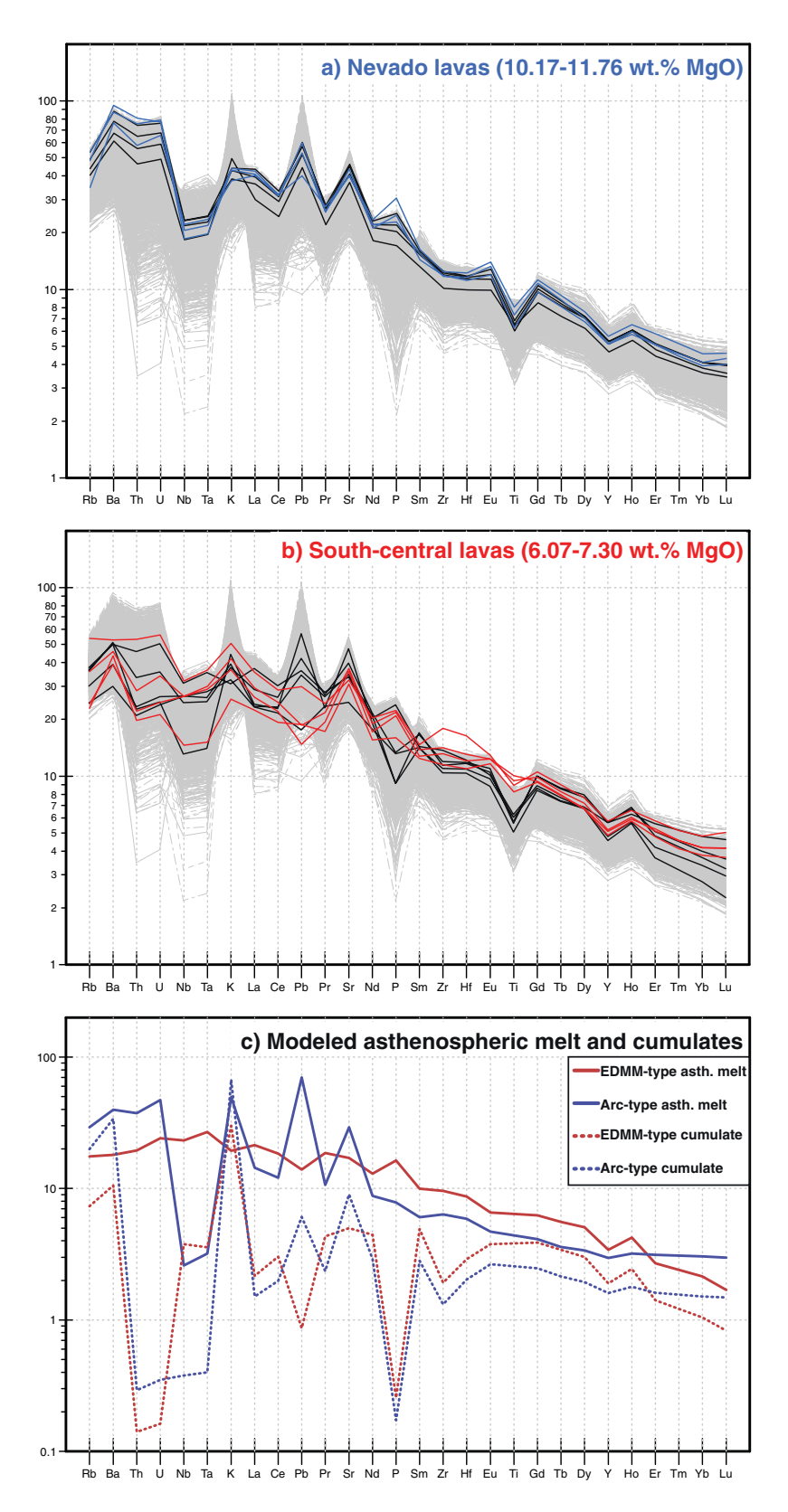


Figure 15. Primitive mantle-normalized trace element diagram displaying model results vs. representative Payenia sample compositions. (a) Blue lines represent selected samples from the Nevado area and (b) red lines represent samples from the south-central area. Gray lines represent 2000 random mixtures between the asthenospheric melt, the modeled melts of the EDMM-type SCLM source, and the modeled melts of the arc-type SCLM source. Thin black lines are selected modeled melt mixtures that resemble representative Payenia melt compositions. (c) Trace element patterns for modeled asthenospheric melt (solid lines) and SCLM cumulate (dashed lines).

CHILSON-PARKS ET AL. 25 of 32



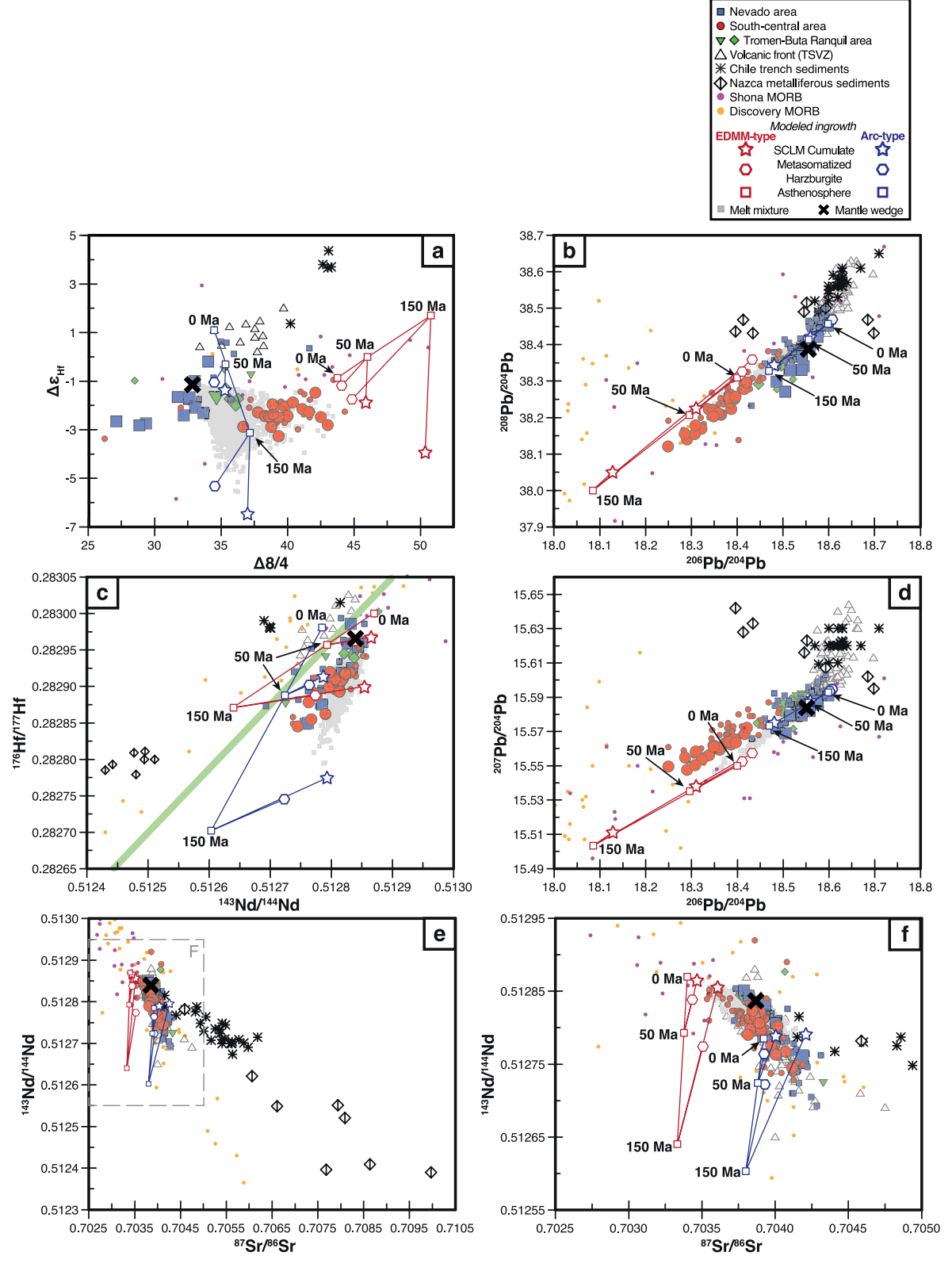


Figure 16.

CHILSON-PARKS ET AL. 26 of 32



Although we highlight the compositional similarity between Payenia lavas and melt pocket-bearing mantle xenoliths from Patagonia, the mantle xenoliths that do occur in the eastern margin of Payenia at the Agua Poca locality lack the hydrous metasomatic phases that we predict in our model (Bertotto et al., 2013). Unfortunately, there are very few localities with mantle xenoliths and they tend to be far removed to the east of the regions affected by subduction processes. Metasomatized xenoliths with and without hydrous phases have been observed in Patagonia south of Payenia (e.g., Bjerg et al., 2005; Dantas et al., 2009; Jalowitzki et al., 2017; Rivalenti et al., 2007). The lack of hydrous cumulates may result from melting of the SCLM to such a degree that the hydrous phases were consumed, as has been suggested for mantle xenoliths from Australia (Yaxley & Kamenetsky, 1999), and the glass veins found in the Agua Poca xenoliths may have compositions that exhibit this hydrous cumulate signature without hydrous phases present. The lack of mantle xenoliths underscores the importance of using basalt samples to identify and characterize the signal of SCLM in continental subduction magmatism.

An important link may exist between melt percolation, crystallization, and metasomatism of the SCLM and the oxygen isotope signature of alkali basalts produced during melting of the SCLM. Specifically, contributions from the metasomatized lithospheric mantle may lower δ^{18} O values in mafic melt, warranting a reconsideration of low- δ^{18} O values previously observed in lavas that have the lithospheric mantle as a source. Multiple localities outside of Payenia have yielded geochemical observations that are compatible with the implications of our model results. Metasomatized lherzolite and pyroxenite xenoliths from the Colorado Plateau yield pyroxene δ^{18} O values that are on average about 0.5% lower than typical peridotite values of 5.5 and 5.7% for clinopyroxene and orthopyroxene, respectively (Perkins et al., 2006). The Horoman peridotite massif of northern Japan shows evidence of melt metasomatism yielding whole-rock δ^{18} O values of 5.0-5.7% (Ranaweera et al., 2018), a range lower than the low end of typical peridotite values ($5.5 \pm 0.2\%$); Eiler, 2001). Olivine and orthopyroxene grains in metasomatized polymict xenoliths from the Kaapvaal craton yield δ^{18} O values over 1% lower than those measured from of Kaapvaal peridotite xenoliths, whose δ^{18} O values are representative of the "average mantle" range (Zhang et al., 2000). As is demonstrated in our model, mineral phases such as amphibole and clinopyroxene, which occur in metasomatized SCLM, retain lighter oxygen isotopes relative to the crystallizing melt at temperatures typical of the SCLM. When compared to $\delta^{18}O_{\text{olivine}}$ values from other continental arc settings, Payenia lavas display a smaller range in $\delta^{18}O_{olivine}$, lacking $\delta^{18}O_{olivine}$ values above mantle values, as is observed in basalts from the VF of Kamchatka (4.5–7.4%; Bindeman et al., 2004; Auer et al., 2009), VF and back-arc volcanoes in Central America (δ¹⁸O_{oli}, vine = 4.6-5.7%; Eiler et al., 2005), and arc volcanoes located at variable distances from the trench in Mexico $(\delta^{18}O_{\text{olivine}} = 5.3 - 6.6\%)$; Johnson et al., 2009; Straub et al., 2015), and the Cascades $(\delta^{18}O_{\text{olivine}} = 4.7 - 6.1\%)$ Martin et al., 2011). Our model results demonstrate that relatively light oxygen isotopes in mafic volcanism in continental back-arc and continental intraplate settings can be inherited from SCLM that received little to no input from low-18O melts.

5. Conclusions

The main conclusions are as follows:

- 1. Although we cannot disprove that crustal contamination played some role in the composition of some Payenia lavas, current observations indicate that crustal contamination was not the dominant factor controlling the composition of the Payenia lavas.
- 2. Major trace element and isotopes systematics demonstrate that the Buta Ranquil area lavas display a compositional range caused by mixing of 60%–80% of melt resembling the south-central lavas with 20%–40% of lavas from the Tromen stratovolcano.

Figure 16. Modeled isotopic ingrowth estimates in comparison to natural samples from Payenia. Lines represent the isotopic evolution of the arc- (blue) and EDMM-type (red) asthenosphere mantle (open squares), from which the melts that metasomatize the SCLM originate. SCLM cumulate (open stars) and metasomatized harzburgite (open hexagons) represent the modeled present-day isotope ratios for SCLM cumulate and metasomatize harzburgites, respectively, after experiencing 50 and 150 million years of isotopic ingrowth. Age labels next to the squares represent the time at which isotopic ingrowth in the SCLM commenced. Gray squares represent the modeled present-day mixtures between SCLM melts, which inherit the cumulate and metasomatized harzburgite isotope ratios, and the estimated mantle wedge melt (black X). Panel f has the same bounds as the gray dashed box in panel e. Symbols for VF lavas, Chile trench sediments, Nazca Plate metalliferous sediments, MORB samples from the Shona and Discovery MAR segments, and the mantle Hf-Nd isotope array are the same as in Figure 5.

CHILSON-PARKS ET AL. 27 of 32



Acknowledgments

This work serves as a testament to the

Frey. Their curiosity, generosity, and

lives of Fernando Calabozo and Frederick

diligence continue to benefit and be cel-

ebrated by their collaborators. This work

was supported by NSF EAR 0810191

to Alberto E. Saal and FONCyT: PICT

RAÍCES #265 and SECyT-UNC grants

E. Saal. We thank Brad Erkkila (Yale)

for instrumentation assistance and Kei

Shimizu (University of Wisconsin-Mad-

ison) and Paula Antoshechkina (Caltech)

for assistance with use of alphaMELTS.

Finally, we extend our sincere gratitude

one anonymous reviewer for thoughtful

to Charles Stern, Sebastian Pilet and

and constructive reviews that greatly

improved our manuscript.

awarded to Ivan A. Petrinovic and Alberto

- 3. The major and trace element concentrations and isotope ratios presented in this study suggest that the SCLM metasomatized 50–150 Ma by two different types of melts: one generated from an Discovery-Shona MORB source and another that was influenced by melts generated from the mantle-wedge during subduction zone processes have played a significant role in the composition of Payena lavas. Model results suggest that the SCLM metasomatism is linked to two Mesozoic events: the breakup of Gondwana and the development the proto-Pacific convergent margin in northern Patagonia. The subsequent melting of the metasomatized SCLM would have been caused by thinning and heating experienced beneath Payenia during post-Miocene changes in subduction geometry.
- 4. The composition of lavas affected by metasomatized SCLM underscores the possibility that arc basalts can acquire low $\delta^{18}O_{\text{olivine}}$ values not only from ^{18}O -depleted fluids released from the downgoing slab, but also from the oxygen isotope fractionations that occur during fractional crystallization of melts and formation vein-cumulate in SCLM.
- 5. The SCLM signal recorded in Payenia lavas demonstrates the potential for basaltic back-arc lavas to elucidate the origins and timing of fluxes traveling from the convecting mantle into the lithospheric mantle.

Data Availability Statement

The geochemical data used for this research are archived at the public domain repository OSF: https://osf. io/9jes6/?view_only=bbf6bad300bf493897547d0b8675cecf.

References

- Abre, P., Cingolani, C. A., & Manassero, M. J. (2017). The Pavón formation as the upper Ordovician unit developed in a turbidite sand-rich ramp. San Rafael block, Mendoza, Argentina. In *Pre-carboniferous evolution of the San Rafael Block* (pp. 87–104). Springer. https://doi.org/10.1007/978-3-319-50153-6 5
- Aliani, P., Ntaflos, T., & Bjerg, E. (2009). Origin of melt pockets in mantle xenoliths from southern Patagonia, Argentina. *Journal of South American Earth Sciences*, 28(4), 419–428. https://doi.org/10.1016/j.jsames.2009.04.009
- Andres, M., Blichert-Toft, J., & Schilling, J.-G. (2002). Hafnium isotopes in basalts from the southern Mid-Atlantic Ridge from 40°S to 55°S: Discovery and Shona plume-ridge interactions and the role of recycled sediments. *Geochemistry, Geophysics, Geosystems*, 3(10), 1–25. https://doi.org/10.1029/2002gc000324
- Angermann, D., Klotz, J., & Reigber, C. (1999). Space-geodetic estimation of the Nazca-South America Euler vector. Earth and Planetary Science Letters, 171(3), 329–334. https://doi.org/10.1016/s0012-821x(99)00173-9
- Asimow, P. D., Dixon, J., & Langmuir, C. (2004). A hydrous melting and fractionation model for mid-ocean ridge basalts: Application to the Mid-Atlantic Ridge near the Azores. *Geochemistry, Geophysics, Geosystems*, 5(1), Q01E16. https://doi.org/10.1029/2003gc000568
- Auer, S., Bindeman, I., Wallace, P., Ponomareva, V., & Portnyagin, M. (2009). The origin of hydrous, high-618O voluminous volcanism: Diverse oxygen isotope values and high magmatic water contents within the volcanic record of Klyuchevskoy volcano, Kamchatka, Russia. Contributions to Mineralogy and Petrology, 157(2), 209–230. https://doi.org/10.1007/s00410-008-0330-0
- Bertotto, G. W., Bjerg, E. A., & Cingolani, C. A. (2006). Hawaiian and Strombolian style monogenetic volcanism in the extra-Andean domain of central-west Argentina. *Journal of Volcanology and Geothermal Research*, 158(3), 430–444. https://doi.org/10.1016/j.jvolgeores.2006.08.001
 Bertotto, G. W., Mazzucchelli, M., Zanetti, A., & Vannucci, R. (2013). Petrology and geochemistry of the back-arc lithospheric mantle beneath eastern Payunia (La Pampa, Argentina): Evidence from Agua Poca peridotite xenoliths. *Geochemical Journal*, 47(2), 219–234. https://doi.org/10.2343/geochemj.2.0256
- Bindeman, I. N., Ponomareva, V. V., Bailey, J. C., & Valley, J. W. (2004). Volcanic arc of Kamchatka: A province with high-818O magma sources and large-scale 18O/16O depletion of the upper crust. *Geochimica et Cosmochimica Acta*, 68(4), 841–865. https://doi.org/10.1016/j.gca.2003.07.009
- Bjerg, E. A., Ntaflos, T., Kurat, G., Dobosi, G., & Labudia, C. H. (2005). The upper mantle beneath Patagonia, Argentina, documented by xeno-liths from alkali basalts. *Journal of South American Earth Sciences*, 18(2), 125–145. https://doi.org/10.1016/j.jsames.2004.09.002
- Bucholz, C. E., Jagoutz, O., VanTongeren, J. A., Setera, J., & Wang, Z. (2017). Oxygen isotope trajectories of crystallizing melts: Insights from modeling and the plutonic record. *Geochimica et Cosmochimica Acta*, 207, 154–184. https://doi.org/10.1016/j.gca.2017.03.027
- Burd, A. I., Booker, J. R., Mackie, R., Favetto, A., & Pomposiello, M. C. (2014). Three-dimensional electrical conductivity in the mantle beneath the Payún Matrú Volcanic field in the Andean backarc of Argentina near 36.5°S: Evidence for decapitation of a mantle plume by resurgent upper mantle shear during slab steepening. *Geophysical Journal International*, 198(2), 812–827. https://doi.org/10.1093/gji/ggu145
- Chauvel, C., Lewin, E., Carpentier, M., Arndt, N. T., & Marini, J.-C. (2008). Role of recycled oceanic basalt and sediment in generating the Hf–Nd mantle array. *Nature Geoscience*, 1(1), 64–67. https://doi.org/10.1038/ngeo.2007.51
- Cingolani, C. A., Basei, M. A. S., Varela, R., Llambías, E. J., Chemale, F., Abre, P., et al. (2017). The mesoproterozoic basement at the san Rafael block, Mendoza Province (Argentina): Geochemical and isotopic age constraints. In *Pre-carboniferous evolution of the San Rafael Block* (pp. 19–58), https://doi.org/10.1007/978-3-319-50153-6 2
- Cingolani, C. A., Llambías, E. J., Basei, M. A., Uriz, N. J., Chemale, F., & Abre, P. (2017). The Rodeo de la Bordalesa Tonalite Dykes as a lower Devonian magmatic event: Geochemical and isotopic age constraints. In *Pre-carboniferous evolution of the San Rafael Block* (pp. 221–238). Springer. https://doi.org/10.1007/978-3-319-50153-6_12
- Cingolani, C. A., Llambías, E. J., Chemale, F., Abre, P., & Uriz, N. J. (2017). Lower Paleozoic 'El Nihuil Dolerites': Geochemical and isotopic constraints of mafic magmatism in an extensional setting of the san Rafael block, Mendoza, Argentina. In *Pre-carboniferous evolution of the San Rafael Block* (pp. 105–125). Springer. https://doi.org/10.1007/978-3-319-50153-6_6

CHILSON-PARKS ET AL. 28 of 32



- Condamine, P., & Médard, E. (2014). Experimental melting of phlogopite-bearing mantle at 1 GPa: Implications for potassic magmatism. *Earth and Planetary Science Letters*, 397, 80–92. https://doi.org/10.1016/j.epsl.2014.04.027
- Dantas, C., Grégoire, M., Koester, E., Conceição, R. V., & Rieck, N. (2009). The lherzolite-websterite xenolith suite from Northern Patagonia (Argentina): Evidence of mantle-melt reaction processes. *Lithos*, 107(1), 107–120. https://doi.org/10.1016/j.lithos.2008.06.012
- Davidson, J. P., Dungan, M. A., Ferguson, K. M., & Colucci, M. T. (1987). Crust-magma interactions and the evolution of arc magmas: The San Pedro–Pellado volcanic complex, southern Chilean Andes. *Geology*, 15(5), 443–446. https://doi.org/10.1130/0091-7613(1987)15<443:ciateo>2.0.co; 2
- Davidson, J. P., Ferguson, K. M., Colucci, M. T., & Dungan, M. A. (1988). The origin and evolution of magmas from the san Pedro-Pellado volcanic complex, S. Chile: Multicomponent sources and open system evolution. *Contributions to Mineralogy and Petrology*, 100(4), 429–445. Journal article. https://doi.org/10.1007/bf00371373
- Dekov, V. M., Cuadros, J., Kamenov, G. D., Weiss, D., Arnold, T., Basak, C., & Rochette, P. (2010). Metalliferous sediments from the HMS Challenger voyage (1872–1876). Geochimica et Cosmochimica Acta, 74(17), 5019–5038. https://doi.org/10.1016/j.gca.2010.06.001
- Dixon, J. E., Leist, L., Langmuir, C., & Schilling, J.-G. (2002). Recycled dehydrated lithosphere observed in plume-influenced mid-ocean-ridge basalt. *Nature*, 420(6914), 385. https://doi.org/10.1038/nature01215
- Douglass, J., Schilling, J.-G., & Fontignie, D. (1999). Plume-ridge interactions of the Discovery and Shona mantle plumes with the southern Mid-Atlantic Ridge (40°–55°S). *Journal of Geophysical Research: Solid Earth*, 104(B2), 2941–2962. https://doi.org/10.1029/98jb02642
- Dungan, M. A., Wulff, A., & Thompson, R. (2001). Eruptive stratigraphy of the Tatara–San Pedro complex, 36 S, southern Volcanic zone, Chilean Andes: Reconstruction method and implications for magma evolution at long-lived arc volcanic centers. *Journal of Petrology*, 42(3), 555–626. https://doi.org/10.1093/petrology/42.3.555
- Dyhr, C. T., Holm, P. M., & Llambías, E. J. (2013). Geochemical constraints on the relationship between the Miocene–Pliocene volcanism and tectonics in the Palaoco and fortunoso volcanic fields, Mendoza region, Argentina: New insights from 40 Ar/39 Ar dating, Sr–Nd–Pb isotopes and trace elements. *Journal of Volcanology and Geothermal Research*, 266, 50–68. https://doi.org/10.1016/j.jvolgeores.2013.08.005
- Dyhr, C. T., Holm, P. M., Llambías, E. J., & Scherstén, A. (2013). Subduction controls on Miocene back-arc lavas from Sierra de Huantraico and La Matancilla and new 40 Ar/39 Ar dating from the Mendoza region, Argentina. Lithos, 179, 67–83. https://doi.org/10.1016/j.lithos.2013.08.007
- Eiler, J. M. (2001). Oxygen isotope variations of basaltic lavas and upper mantle rocks. *Reviews in Mineralogy and Geochemistry*, 43(1), 319–364. https://doi.org/10.2138/gsrmg.43.1.319
- Eiler, J. M., Carr, M. J., Reagan, M., & Stolper, E. (2005). Oxygen isotope constraints on the sources of Central American arc lavas. *Geochemistry, Geophysics, Geosystems*, 6(7), Q07007. https://doi.org/10.1029/2004gc000804
- Eiler, J. M., Crawford, A., Elliott, T., Farley, K. A., Valley, J. W., & Stolper, E. M. (2000). Oxygen isotope geochemistry of oceanic-arc lavas. *Journal of Petrology*, 41(2), 229–256. https://doi.org/10.1093/petrology/41.2.229
- Eiler, J. M., Schiano, P., Kitchen, N., & Stolper, E. M. (2000). Oxygen-isotype evidence for recycled crust in the sources of mid-ocean-ridge basalts. *Nature*. 403(6769), 530–534. https://doi.org/10.1038/35000553
- Eiler, J. M., Valley, J. W., & Stolper, E. M. (1996). Oxygen isotope ratios in olivine from the Hawaii scientific drilling Project. *Journal of Geo-physical Research*, 101(B5), 11807–11811. https://doi.org/10.1029/95jb03194
- Espanon, V. R., Chivas, A. R., Kinsley, L. P. J., & Dosseto, A. (2014). Geochemical variations in the Quaternary Andean back-arc volcanism,
- southern Mendoza, Argentina. *Lithos*, 208, 251–264. https://doi.org/10.1016/j.lithos.2014.09.010

 Ferguson, K. M., Dungan, M. A., Davidson, J. P., & Colucci, M. T. (1992). The Tatara–San Pedro Volcano, 36 S, Chile: A chemically variable, dominantly mafic magmatic system. *Journal of Petrology*, 33(1), 1–43. https://doi.org/10.1093/petrology/33.1.1
- Foley, S. (1992). Vein-plus-wall-rock melting mechanisms in the lithosphere and the origin of potassic alkaline magmas. *Lithos*, 28(3–6), 435–453. https://doi.org/10.1016/0024-4937(92)90018-t
- Folguera, A., Naranjo, J. A., Orihashi, Y., Sumino, H., Nagao, K., Polanco, E., & Ramos, V. A. (2009). Retroarc volcanism in the northern san Rafael block (34–35 30' S), southern central Andes: Occurrence, age, and tectonic setting. *Journal of Volcanology and Geothermal Research*, 186(3), 169–185. https://doi.org/10.1016/j.jvolgeores.2009.06.012
- Franzese, J., Spalletti, L., Pérez, I. G., & Macdonald, D. (2003). Tectonic and paleoenvironmental evolution of Mesozoic sedimentary basins along the Andean foothills of Argentina (32–54 S). *Journal of South American Earth Sciences*, 16(1), 81–90. https://doi.org/10.1016/s0895-9811(03)00020-8
- Gale, A., Dalton, C. A., Langmuir, C. H., Su, Y., & Schilling, J.-G. (2013). The mean composition of ocean ridge basalts. Geochemistry, Geo-physics, Geosystems, 14(3), 489–518. https://doi.org/10.1029/2012gc004334
- Germa, A., Quidelleur, X., Gillot, P. Y., & Tchilinguirian, P. (2010). Volcanic evolution of the back-arc Pleistocene Payun Matru volcanic field (Argentina). *Journal of South American Earth Sciences*, 29(3), 717–730. https://doi.org/10.1016/j.jsames.2010.01.002
- Gilbert, H., Beck, S., & Zandt, G. (2006). Lithospheric and upper mantle structure of central Chile and Argentina. *Geophysical Journal International*, 165(1), 383–398. https://doi.org/10.1111/j.1365-246x.2006.02867.x
- Gordon, A., & Ort, M. H. (1993). Edad y correlación del plutonismo subcordillerano en las provincias de Río Negro y Chubut (41–42 30'LS).
 Paper presented at the Congreso Geológico Argentino.
- Gregory, R. T., & Taylor, H. P. (1981). An oxygen isotope profile in a section of Cretaceous oceanic crust, Samail Ophiolite, Oman: Evidence for δ18O buffering of the oceans by deep (>5 km) seawater-hydrothermal circulation at mid-ocean ridges. *Journal of Geophysical Research: Solid Earth* (1978–2012), 86(B4), 2737–2755. https://doi.org/10.1029/jb086ib04p02737
- Gudnason, J., Holm, P. M., Søager, N., & Llambías, E. J. (2012). Geochronology of the late Pliocene to recent volcanic activity in the Payenia back-arc volcanic province, Mendoza Argentina. *Journal of South American Earth Sciences*, 37(0), 191–201. https://doi.org/10.1016/j.isames.2012.02.003
- Haller, M. J., & Lapido, O. R. (1980). El Mesozoico de la Cordillera Patagónica central. Revista de la Asociación Geológica Argentina, 35(2), 230–247.
- Harmon, R. S., Barreiro, B. A., Moorbath, S., Hoefs, J., Francis, P. W., Thorpe, R. S., et al. (1984). Regional O-, Sr-, and Pb-isotope relationships in late Cenozoic calc-alkaline lavas of the Andean Cordillera. *Journal of the Geological Society*, 141(5), 803–822. https://doi.org/10.1144/ gsigs.141.5.0803
- Hart, S. R. (1984). A large-scale isotope anomaly in the Southern Hemisphere mantle. *Nature*, 309, 753–757. https://doi.org/10.1038/309753a0 Hernando, I., Aragón, E., Frei, R., González, P., & Spakman, W. (2014). Constraints on the origin and evolution of magmas in the Payún Matrú Volcanic field, quaternary Andean Back-arc of Western Argentina. *Journal of Petrology*, 55(1), 209–239. https://doi.org/10.1093/petrology/egt066
- Hickey, R. L., Frey, F. A., Gerlach, D. C., & Lopez-Escobar, L. (1986). Multiple sources for basaltic arc rocks from the southern volcanic zone of the Andes (34–41°S): Trace element and isotopic evidence for contributions from subducted oceanic crust, mantle, and continental crust. *Journal of Geophysical Research: Solid Earth* (1978–2012), 91(B6), 5963–5983. https://doi.org/10.1029/jb091ib06p05963

CHILSON-PARKS ET AL. 29 of 32



- Hickey-Vargas, R., Holbik, S., Tormey, D., Frey, F. A., & Moreno Roa, H. (2016). Basaltic rocks from the Andean Southern Volcanic Zone: Insights from the comparison of along-strike and small-scale geochemical variations and their sources. *Lithos*, 258, 115–132. https://doi.org/10.1016/j.lithos.2016.04.014
- Hickey-Vargas, R., Sun, M., & Holbik, S. (2016). Geochemistry of basalts from small eruptive centers near Villarrica stratovolcano, Chile: Evidence for lithospheric mantle components in continental arc magmas. Geochimica et Cosmochimica Acta, 185, 358–382. https://doi.org/10.1016/j.gca.2016.03.033
- Hildreth, W., & Moorbath, S. (1988). Crustal contributions to arc magmatism in the Andes of central Chile. *Contributions to Mineralogy and Petrology*, 98(4), 455–489. https://doi.org/10.1007/bf00372365
- Holm, P. M., Søager, N., Alfastsen, M., & Bertotto, G. W. (2016). Subduction zone mantle enrichment by fluids and Zr-Hf-depleted crustal melts as indicated by backarc basalts of the Southern Volcanic Zone, Argentina. Lithos, 262, 135–152. https://doi.org/10.1016/j.lithos.2016.06.029
- Holm, P. M., Søager, N., Dyhr, C. T., & Nielsen, M. R. (2014). Enrichments of the mantle sources beneath the Southern Volcanic Zone (Andes) by fluids and melts derived from abraded upper continental crust. Contributions to Mineralogy and Petrology, 167(5), 1–27. https://doi.org/10.1007/s00410-014-1004-8
- Jacques, G., Hoernle, K., Gill, J., Hauff, F., Wehrmann, H., Garbe-Schönberg, D., et al. (2013). Across-arc geochemical variations in the southern Volcanic zone, Chile (34.5–38.0°S): Constraints on mantle wedge and slab input compositions. *Geochimica et Cosmochimica Acta*, 123, 218–243
- Jalowitzki, T., Gervasoni, F., Conceição, R. V., Orihashi, Y., Bertotto, G. W., Sumino, H., et al. (2017). Slab-derived components in the subcontinental lithospheric mantle beneath Chilean Patagonia: Geochemistry and Sr-Nd-Pb isotopes of mantle xenoliths and host basalt. Lithos, 292-293, 179-197. https://doi.org/10.1016/j.lithos.2017.09.008
- Johnson, D. M., Hooper, P. R., & Conrey, R. M. (1999). XRF analysis of rocks and minerals for major and trace elements on a single low dilution Li-tetraborate fused bead. In *Paper presented at the advances in X-ray analysis* (Vol. 41, pp. 843–867).
- Johnson, E. R., Wallace, P. J., Delgado Granados, H., Manea, V. C., Kent, A. J. R., Bindeman, I. N., & Donegan, C. S. (2009). Subduction-related volatile recycling and magma generation beneath Central Mexico: Insights from melt inclusions, oxygen isotopes and geodynamic models. *Journal of Petrology*, 50(9), 1729–1764. https://doi.org/10.1093/petrology/egp051
- Kay, S. M., Burns, W. M., Copeland, P., & Mancilla, O. (2006). Upper Cretaceous to Holocene magmatism and evidence for transient Miocene shallowing of the Andean subduction zone under the northern Neuquén Basin. Geological Society of America Special Paper, 407, 19–60. https://doi.org/10.1130/2006.2407(02)
- Kay, S. M., & Copeland, P. (2006). Early to middle Miocene backarc magmas of the Neuquén Basin: Geochemical consequences of slab shallowing and the westward drift of South America. Geological Society of America Special Paper, 407, 185–213. https://doi.org/10.1130/2006.2407(09)
- Kay, S. M., Gorring, M., & Ramos, V. A. (2004). Fuentes magmáticas, ambientes y causas del magmatismo de plateau Eoceno a Reciente en la Patagonia (36°S a 52°S latitud). Revista de la Asociación Geológica Argentina, 59(4), 556–568.
- Kay, S. M., Jones, H. A., & Kay, R. W. (2013). Origin of Tertiary to Recent EM-and subduction-like chemical and isotopic signatures in Auca Mahuida region (37–38°S) and other Patagonian plateau lavas. Contributions to Mineralogy and Petrology, 166(1), 165–192. https://doi.org/10.1007/s00410-013-0870-9
- Kay, S. M., Mancilla, O., & Copeland, P. (2006). Evolution of the late Miocene Chachahuén volcanic complex at 37°S over a transient shallow subduction zone under the Neuquén Andes. Geological Society of America Special Paper, 407, 215–246. https://doi.org/10.1130/2006.2407(10)
- Kay, S. M., Orrell, S., & Abbruzzi, J. (1996). Zircon and whole rock Nd-Pb isotopic evidence for a Grenville age and a Laurentian origin for the basement of the Precordillera in Argentina. The Journal of Geology, 104, 637–648. https://doi.org/10.1086/629859
- Kendrick, E., Bevis, M., Smalley, R., Brooks, B., Vargas, R. B., Lauria, E., & Fortes, L. P. S. (2003). The Nazca–South America Euler vector and its rate of change. *Journal of South American Earth Sciences*, 16(2), 125–131. https://doi.org/10.1016/s0895-9811(03)00028-2
- Kilian, R., & Stern, C. R. (2002). Constraints on the interaction between slab melts and the mantle wedge from adakitic glass in peridotite xeno-liths. European Journal of Mineralogy, 14(1), 25–36. https://doi.org/10.1127/0935-1221/2002/0014-0025
- Laurora, A., Mazzucchelli, M., Rivalenti, G., Vannucci, R., Zanetti, A., Barbieri, M. A., & Cingolani, C. A. (2001). Metasomatism and melting in carbonated peridotite xenoliths from the mantle wedge: The Gobernador Gregores case (southern Patagonia). *Journal of Petrology*, 42(1), 69–87. https://doi.org/10.1093/petrology/42.1.69
- Le Bas, M. J., Le Maitre, R. W., Streckeisen, A., & Zanettin, B. (1986). A chemical classification of volcanic rocks based on the total alkali-silica diagram. *Journal of Petrology*, 27(3), 745–750. https://doi.org/10.1093/petrology/27.3.745
- Lee, C.-T. A., & Bachmann, O. (2014). How important is the role of crystal fractionation in making intermediate magmas? Insights from Zr and P systematics. Earth and Planetary Science Letters, 393, 266–274. https://doi.org/10.1016/j.epsl.2014.02.044
- Lizuain, A. (1999). Estratigrafía y evolución geológica del Jurásico y Cretácico de la Cordillera Patagónica septentrional. In G. Argentina, & R. Caminos (Eds.), Subsecretaría de Minería de la Nación, servicio geológico minero Argentino (Vol. 29, pp. 433–556). Instituto de Geología y Recursos Minerales, Anales.
- Lucassen, F., Trumbull, R., Franz, G., Creixell, C., Vásquez, P., Romer, R. L., & Figueroa, O. (2004). Distinguishing crustal recycling and juvenile additions at active continental margins: The Paleozoic to recent compositional evolution of the Chilean Pacific margin (36–41°S). *Journal of South American Earth Sciences*, 17(2), 103–119. https://doi.org/10.1016/j.jsames.2004.04.002
- Lucassen, F., Wiedicke, M., & Franz, G. (2010). Complete recycling of a magmatic arc: Evidence from chemical and isotopic composition of quaternary Trench sediments in Chile (36°–40°S). *International Journal of Earth Sciences*, 99(3), 687–701. https://doi.org/10.1007/s00531-008-0410-4
- MacDonald, G. A., & Katsura, T. (1964). Chemical composition of Hawaiian lavas1. Journal of Petrology, 5(1), 82–133. https://doi.org/10.1093/petrology/5.1.82
- Martin, E., Bindeman, I., & Grove, T. (2011). The origin of high-Mg magmas in Mt Shasta and medicine Lake volcanoes, Cascade arc (California): Higher and lower than mantle oxygen isotope signatures attributed to current and past subduction. Contributions to Mineralogy and Petrology, 162(5), 945–960. https://doi.org/10.1007/s00410-011-0633-4
- Mattey, D., Lowry, D., & Macpherson, C. (1994). Oxygen isotope composition of mantle peridotite. Earth and Planetary Science Letters, 128(3), 231–241. https://doi.org/10.1016/0012-821x(94)90147-3
- McDonough, W. F., & Sun, S. S. (1995). The composition of the Earth. Chemical Geology, 120(3), 223–253. https://doi.org/10.1016/0009-2541(94)00140-4
- Pallares, C., Quidelleur, X., Gillot, P.-Y., Kluska, J.-M., Tchilinguirian, P., & Sarda, P. (2016). The temporal evolution of back-arc magmas from the Auca Mahuida shield volcano (Payenia Volcanic Province, Argentina). *Journal of Volcanology and Geothermal Research*, 323, 19–37. https://doi.org/10.1016/j.jvolgeores.2016.04.043

CHILSON-PARKS ET AL. 30 of 32



- Perkins, G. B., Sharp, Z. D., & Selverstone, J. (2006). Oxygen isotope evidence for subduction and rift-related mantle metasomatism beneath the Colorado Plateau–Río Grande rift transition. *Contributions to Mineralogy and Petrology*, 151(6), 633–650. https://doi.org/10.1007/s00410-006-0075-6
- Pilet, S., Baker, M. B., Müntener, O., & Stolper, E. M. (2011). Monte Carlo simulations of metasomatic enrichment in the lithosphere and implications for the source of alkaline basalts. *Journal of Petrology*, 52(7–8), 1415–1442. https://doi.org/10.1093/petrology/egr007
- Pilet, S., Baker, M. B., & Stolper, E. M. (2008). Metasomatized lithosphere and the origin of alkaline lavas. Science, 320(5878), 916–919. https://doi.org/10.1126/science.1156563
- Ramos, V. (1999). Plate tectonic setting of the Andean Cordillera. Episodes, 22, 183-190. https://doi.org/10.18814/epiiugs/1999/v22i3/005
- Ramos, V. A. (2004). Cuyania, an exotic block to Gondwana: Review of a historical success and the present Problems. *Gondwana Research*, 7(4), 1009–1026. https://doi.org/10.1016/s1342-937x(05)71081-9
- Ramos, V. A. (2005). Seismic ridge subduction and topography: Foreland deformation in the Patagonian Andes. *Tectonophysics*, 399(1), 73–86. https://doi.org/10.1016/j.tecto.2004.12.016
- Ramos, V. A. (2009). Anatomy and global context of the Andes: Main geologic features and the Andean orogenic cycle. In *Backbone of the Americas: Shallow subduction, plateau uplift, and ridge and terrane collision*. https://doi.org/10.1130/2009.1204(02)
- Ramos, V. A. (2010). The Grenville-age basement of the Andes. Journal of South American Earth Sciences, 29(1), 77–91. https://doi.org/10.1016/j.jsames.2009.09.004
- Ramos, V. A., & Folguera, A. (2011). Payenia volcanic province in the Southern Andes: An appraisal of an exceptional Quaternary tectonic setting. *Journal of Volcanology and Geothermal Research*, 201(1), 53–64. https://doi.org/10.1016/j.jvolgeores.2010.09.008
- Ranaweera, L. V., Ota, T., Moriguti, T., Tanaka, R., & Nakamura, E. (2018). Circa 1 Ga sub-seafloor hydrothermal alteration imprinted on the Horoman peridotite massif. Scientific Reports, 8(1), 9887. https://doi.org/10.1038/s41598-018-28219-x
- Rivalenti, G., Mazzucchelli, M., Zanetti, A., Vannucci, R., Bollinger, C., Hémond, C., & Bertotto, G. W. (2007). Xenoliths from Cerro de los Chenques (Patagonia): An example of slab-related metasomatism in the backarc lithospheric mantle. *Lithos*, 99(1), 45–67. https://doi. org/10.1016/j.lithos.2007.05.012
- Rodríguez, C., Sellés, D., Dungan, M., Langmuir, C., & Leeman, W. (2007). Adakitic dacites formed by intracrustal crystal fractionation of water-rich parent magmas at Nevado de Longavi volcano (36 2°S; Andean Southern Volcanic Zone, Central Chile). *Journal of Petrology*, 48(11), 2033–2061. https://doi.org/10.1093/petrology/egm049
- 2033–2061. https://doi.org/10.1093/petrology/egm049
 Rowe, M. C., Kent, A. J. R., & Nielsen, R. L. (2009). Subduction influence on oxygen Fugacity and trace and Volatile elements in basalts across the Cascade volcanic arc. *Journal of Petrology*, 50(1), 61–91. https://doi.org/10.1093/petrology/egn072
- Rudnick, R. L., & Gao, S. (2014). 4.1-composition of the continental crust. In H. D. Holland, & K. K. Turekian (Eds.), *Treatise on geochemistry* (2nd ed., pp. 1–51). Elsevier. https://doi.org/10.1016/b978-0-08-095975-7.00301-6
- Ruprecht, P., Bergantz, G. W., Cooper, K. M., & Hildreth, W. (2012). The crustal magma storage system of Volcán Quizapu, Chile, and the effects of magma mixing on magma diversity. *Journal of Petrology*, 53(4), 801–840. https://doi.org/10.1093/petrology/egs002
- Saal, A. E. (1994). Petrology and geochemistry of intra-back arc basalts from the Argentine Andes (M.S. Masters). Massachusetts Institute of Technology.
- Salters, V. J. M., & Stracke, A. (2004). Composition of the depleted mantle. Geochemistry, Geophysics, Geosystems, 5(5), Q05B07. https://doi.org/10.1029/2003gc000597
- Scambelluri, M., Vannucci, R., De Stefano, A., Preite-Martinez, M., & Rivalenti, G. (2009). CO₂ fluid and silicate glass as monitors of alkali basalt/peridotite interaction in the mantle wedge beneath Gobernador Gregores, Southern Patagonia. *Lithos*, 107(1), 121–133. https://doi.org/10.1016/j.lithos.2008.06.015
- Sellés, D., Rodriguez, A., Dungan, M. A., Naranjo, J. A., & Gardeweg, M. (2004). Geochemistry of Nevado de Longaví Volcano (36.2°S): A compositionally atypical arc volcano in the southern Volcanic zone of the Andes. Revista Geologica de Chile. 31(2), 293–315.
- Shimizu, K., Saal, A. E., Myers, C. E., Nagle, A. N., Hauri, E. H., Forsyth, D. W., et al. (2016). Two-component mantle melting-mixing model for the generation of mid-ocean ridge basalts: Implications for the volatile content of the Pacific upper mantle. *Geochimica et Cosmochimica Acta*, 176, 44–80. https://doi.org/10.1016/j.gca.2015.10.033
- Smith, P. M., & Asimow, P. D. (2005). Adiabat_1ph: A new public front-end to the MELTS, pMELTS, and pHMELTS models. *Geochemistry*, *Geophysics*, *Geosystems*, 6(2), Q02004. https://doi.org/10.1029/2004gc000816
- Søager, N., & Holm, P. M. (2013). Melt–peridotite reactions in upwelling eclogite bodies: Constraints from EM1-type alkaline basalts in Payenia, Argentina. Chemical Geology, 360, 204–219. https://doi.org/10.1016/j.chemgeo.2013.10.024
- Søager, N., Holm, P. M., & Llambías, E. J. (2013). Payenia volcanic province, southern Mendoza, Argentina: OIB mantle upwelling in a backarc environment. Chemical Geology, 349–350(0), 36–53. https://doi.org/10.1016/j.chemgeo.2013.04.007
- Søager, N., Holm, P. M., & Thirlwall, M. F. (2015). Sr, Nd, Pb and Hf isotopic constraints on mantle sources and crustal contaminants in the Payenia volcanic province, Argentina. Lithos, 212, 368–378. https://doi.org/10.1016/j.lithos.2014.11.026
- Søager, N., Portnyagin, M., Hoernle, K., Holm, P. M., & Garbe-Schönberg, D. (2018). Constraints on lithosphere-asthenosphere melt mixing in basaltic intraplate volcanism from olivine melt inclusions from southern Payenia, Argentina. *Lithos*, 310, 225–240. https://doi.org/10.1016/j. lithos.2018.04.011
- Søager, N., Portnyagin, M., Hoernle, K., Holm, P. M., Hauff, F., & Garbe-Schönberg, D. (2015). Olivine major and trace element compositions in southern Payenia basalts, Argentina: Evidence for pyroxenite–Peridotite melt mixing in a back-arc setting. *Journal of Petrology*, egv043. https://doi.org/10.1093/petrology/egv043
- Sorbadere, F., Médard, E., Laporte, D., & Schiano, P. (2013). Experimental melting of hydrous peridotite–pyroxenite mixed sources: Constraints on the genesis of silica-undersaturated magmas beneath volcanic arcs. *Earth and Planetary Science Letters*, 384, 42–56. https://doi.org/10.1016/j.epsl.2013.09.026
- Stern, C. R., Frey, F. A., Futa, K., Zartman, R. E., Peng, Z., & Kurtis Kyser, T. (1990). Trace-element and Sr, Nd, Pb, and O isotopic composition of Pliocene and Quaternary alkali basalts of the Patagonian Plateau lavas of southernmost South America. *Contributions to Mineralogy and Petrology*, 104(3), 294–308. https://doi.org/10.1007/bf00321486
- Stern, C. R., Kilian, R., Olker, B., Hauri, E. H., & Kurtis Kyser, T. (1999). Evidence from mantle xenoliths for relatively thin (<100 km) continental lithosphere below the Phanerozoic crust of southernmost South America. *Lithos*, 48(1), 217–235. https://doi.org/10.1016/s0419-0254(99)80013-5
- Straub, S. M., Gómez-Tuena, A., Bindeman, I. N., Bolge, L. L., Brandl, P. A., Espinasa-Perena, R., et al. (2015). Crustal recycling by subduction erosion in the central Mexican Volcanic Belt. *Geochimica et Cosmochimica Acta*, 166, 29–52. https://doi.org/10.1016/j.gca.2015.06.001
- Todt, W., Cliff, R. A., Hanser, A., & Hofmann, A. W. (1996). Evaluation of a 202Pb–205Pb double spike for high-Precision lead isotope analysis. In A. Basu, & S. R. Hart (Eds.), *Earth processes: Reading the isotopic code* (Vol. 95, pp. 429–437). AGU. https://doi.org/10.1029/GM095p0429

CHILSON-PARKS ET AL. 31 of 32



- Tormey, D. R., Frey, F. A., & Lopez-Escobar, L. (1995). Geochemistry of the active Azufre—Planchon—Peteroa Volcanic complex, Chile (35° 15′ S): Evidence for multiple sources and processes in a Cordilleran arc magmatic system. *Journal of Petrology*, 36(2), 265–298. https://doi.org/10.1093/petrology/36.2.265
- Turner, S. J., Langmuir, C. H., Katz, R. F., Dungan, M. A., & Escrig, S. (2016). Parental arc magma compositions dominantly controlled by mantle-wedge thermal structure. *Nature Geoscience*, 9(10), 772. https://doi.org/10.1038/ngeo2788
- Valley, J. W., Kitchen, N., Kohn, M. J., Niendorf, C. R., & Spicuzza, M. J. (1995). UWG-2, a garnet standard for oxygen isotope ratios: Strategies for high precision and accuracy with laser heating. Geochimica et Cosmochimica Acta, 59(24), 5223–5231. https://doi.org/10.1016/0016-7037(95)00386-x
- Wang, J., Hattori, K. H., & Stern, C. R. (2008). Metasomatic origin of garnet orthopyroxenites in the subcontinental lithospheric mantle underlying Pali Aike volcanic field, southern South America. *Mineralogy and Petrology*, 94(3–4), 243–258. https://doi.org/10.1007/s00710-008-0017-2
- Wang, Z., Bucholz, C., Skinner, B., Shimizu, N., & Eiler, J. (2011). Oxygen isotope constraints on the origin of high-Cr garnets from kimberlites. Earth and Planetary Science Letters, 312(3), 337–347. https://doi.org/10.1016/j.epsl.2011.09.061
- Wang, Z., & Eiler, J. M. (2008). Insights into the origin of low-618O basaltic magmas in Hawaii revealed from in situ measurements of oxygen isotope compositions of olivines. Earth and Planetary Science Letters, 269(3), 377–387. https://doi.org/10.1016/j.epsl.2008.02.018
- Watts, K. E., John, D. A., Colgan, J. P., Henry, C. D., Bindeman, I. N., & Valley, J. W. (2019). Oxygen isotopic investigation of silicic magmatism in the Stillwater caldera complex, Nevada: Generation of large-volume, low-818O rhyolitic tuffs and assessment of their regional context in the Great Basin of the western United States. GSA Bulletin, 131(7–8), 1133–1156. https://doi.org/10.1130/b35021.1
- Weller, D. J., & Stern, C. R. (2018). Along-strike variability of primitive magmas (major and volatile elements) inferred from olivine-hosted melt inclusions, southernmost Andean Southern Volcanic Zone, Chile. Lithos, 296, 233–244. https://doi.org/10.1016/j.lithos.2017.11.009
- Workman, R. K., & Hart, S. R. (2005). Major and trace element composition of the depleted MORB mantle (DMM). Earth and Planetary Science Letters, 231(1), 53–72. https://doi.org/10.1016/j.epsl.2004.12.005
- Yaxley, G. M., & Kamenetsky, V. (1999). In situ origin for glass in mantle xenoliths from southeastern Australia: Insights from trace element compositions of glasses and metasomatic phases. Earth and Planetary Science Letters, 172(1-2), 97-109. https://doi.org/10.1016/s0012-821x(99)00196-x
- Zhang, H.-F., Mattey, D. P., Grassineau, N., Lowry, D., Brownless, M., Gurney, J. J., & Menzies, M. A. (2000). Recent fluid processes in the Kaapvaal Craton, South Africa: Coupled oxygen isotope and trace element disequilibrium in polymict peridotites. *Earth and Planetary Science Letters*, 176(1), 57–72. https://doi.org/10.1016/s0012-821x(99)00311-8

CHILSON-PARKS ET AL. 32 of 32